Qeios

Falling Objects and Dust Particles' Motion in the "Collecting Lunar Rock on the Buster Crater" Sequence of the Apollo XVI Footage

ABSTRACT

This manuscript develops and integrates the previous studies "***Analytical Methods for Tracking Bodies Motions on the Lunar Surface in Apollo XVI Footage***" https://doi.org/10.32388/IA8MXE and "***Ballistic motion of dust particles in the "Collecting the Big Muley lunar rock" sequence of the Apollo XVI Footage"*** https://doi.org/10.32388/COXHKG in order to introduce a robust analytical method to trace and analyze the movement of dust shot during the Apollo XVI mission on the lunar surface. By employing both 2D and 3D analysis techniques, we aim to provide a detailed comparison of the observed kinematic events against theoretical models.

The paper extends a previous work focused on the kinematics of lunar dust utilizing footage from the "Grand Prix" sequence of the Apollo XVI mission "Ballistic motion of dust particles in the Lunar Roving Vehicle dust trails" published in 2012 in the American Journal of Physics by Mihaly Horanyi and Hsiang-Wen Hsu: https://www.researchgate.net/publication/258468670 [Ann. 1 – Ann. 2].

In this further analysis, a sequence in which the astronaut Charles Duke collects the Cataclastic Anorthosite 62275 is tracked. There are three significant events that can be traced in this sequence: the vertical fall of a sample bag, the following fall of the Lunar Rock Bags Dispenser and the upward launch of the rock sample that the astronaut is trying to collect. In this last part of the sequence, together with the rock sample, is also possible to trace a certain quantity of lunar dust which is launched with the same initial speed of the rock.

By tracking the falling bodies and the lunar dust, we obtain information about the validity of the expected motion models and about the environment in which the cinematic events took place.

Keywords:

Apollo 16, Lunar dust ballistic motion, Buster Crater, Apollo footage.

https://doi.org/10.32388/RFR2D5

SECTION D

Juggling on the Buster Crater

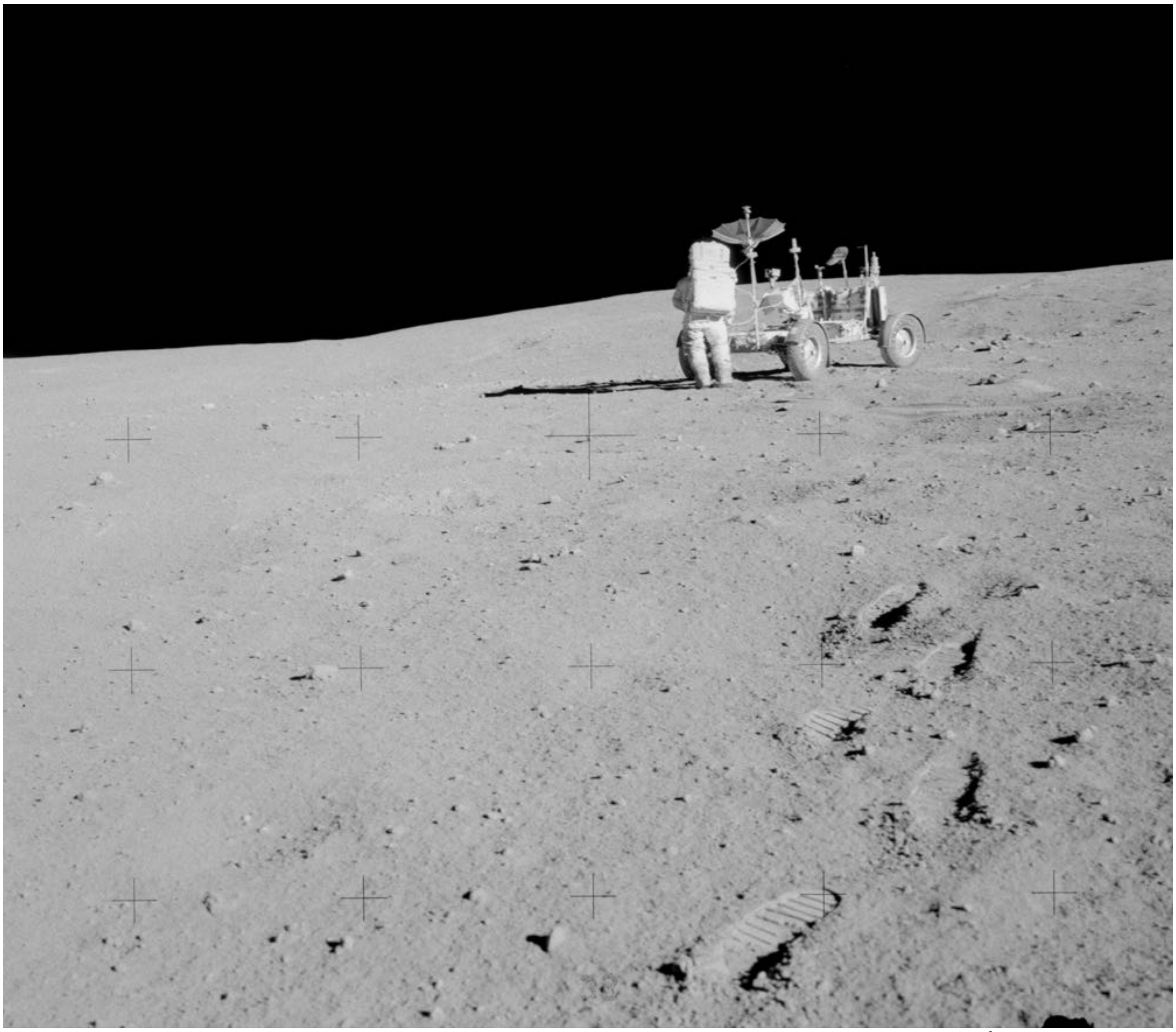

Figure D1 – Eva 1 Station 2, John Young in front of the Rover near Buster Crater [1]

D.1.1 Station 2 - Buster Crater [2]

This station was located about 550 meters west of the LM on the southern rim of Buster Crater. Activities at this stop included a Lunar Portable Magnetometer measurement, panoramic and 500-millimeter photography. Samples were also collected; however, a planned sampling of the rim of nearby Spook Crater was skipped.

---

[1] https://www.hq.nasa.gov/wp-content/uploads/static/history/alsj/a16/AS16-109-17799HR.jpg *Apollo Image Library, Apollo 16 Figure Captions Copyright © 1996-2017 by Eric M. Jones, last revised 16 March 2019.*

[2] https://ntrs.nasa.gov/api/citations/19730013002/downloads/19730013002.pdf *Apollo 16 preliminary science report pag(s) from 6-19 to 6-26, Special Publication NASA-SP-315*

D.1.2 DESCRIPTION OF SEQUENCE [3]

124:39:58 Duke: John, the only trouble is that you can't put the bag...

124:40:00 England: Okay, John, (you can read the LPM).

124:40:00 Duke: ...(lost under Tony).

[Charlie has been holding the bag in his right hand and the scoop in his left. He now transfers the bag to his left hand, leans down to get his right hand on the scoop about half way down the shaft and then runs forward as he lifts the rock with the scoop. The rock flies up off the scoop and Charlie runs forward to try to catch it. He grabs at the rock with his outstretched right hand and manages to bat it up and to his left. He reaches out with his left hand, but his momentum forces him to overshoot and he only manages to bat the rock back to his right. Once again, he almost catches it in his right hand but, finally, the rock falls off-camera to his right. Fendell pans left and, while John does the readings, Charlie gets the scoop under the rock, raises it, tosses it up, steps forward, grabs at it with his right hand and pulls it in against his shoulder. Finally, as he clutches the rock, the sample bag in his left hand falls to the ground.]

124:40:10 Duke: (In the midst of the juggling act) Agh!

124:40:13 Young: Okay: X is 104; Y, 403; Z, 423. (Pause) X, 107; Y, 404; Z, 425. (Pause) X, 110; Y, 405; Z, 425.

[Charlie plants the scoop, transfers the rock to his left hand, and shakes his right hand vigorously to get the dust off.]

124:40:36 England: Okay. Outstanding and visor down (now that the LPM readings are done).

124:40:38 Young: Did you get those (readings), Houston?

124:40:40 England: Sure did.

124:40:42 Young: Visor is down.

[Charlie has the rock in his right hand, again, and has it up close to his faceplate as he examines it.]

124:40:44 Duke: Okay, Tony, the rock I've got here...

[Charlie reaches for another bag but pulls the whole dispenser off. It falls to the ground.]

124:40:47 Young: (LPM) Read switch is Off, and the Power switch is Off.

124:40:52 Duke: (It) is a very friable rock, and it's the most shocked rock I've ever seen; it's just pure white. The whole matrix is pure white. And it's not a breccia. *[This sample is 62275, a 0.43 kg anorthosite.]*

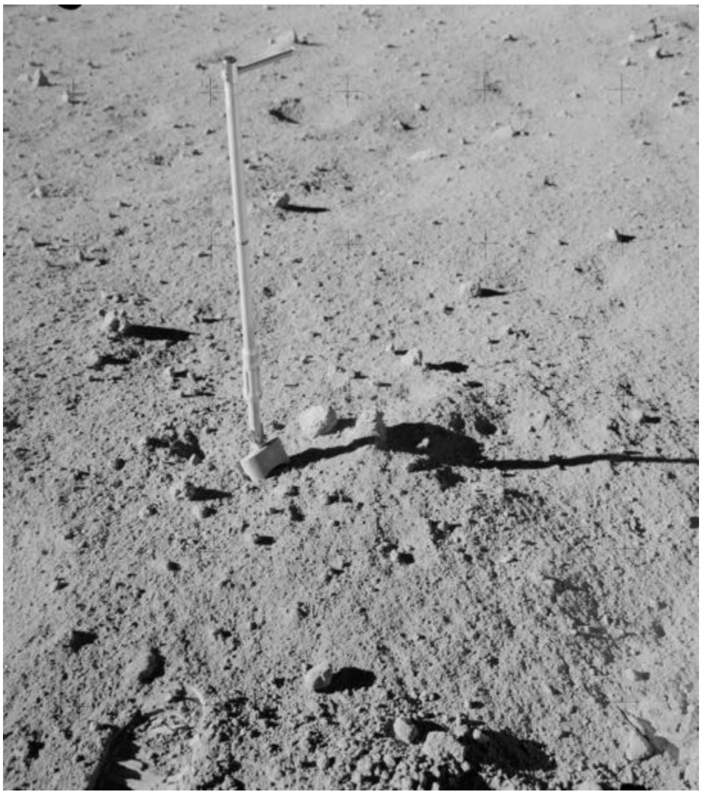

Figure D2 – The site of sample 62275 collection

---

[3] https://www.hq.nasa.gov/alsj/a16/a16.html *Apollo 16 Lunar Surface Journal Corrected Transcript and Commentary by Eric M. Jones. Revised 5 March 2016.*

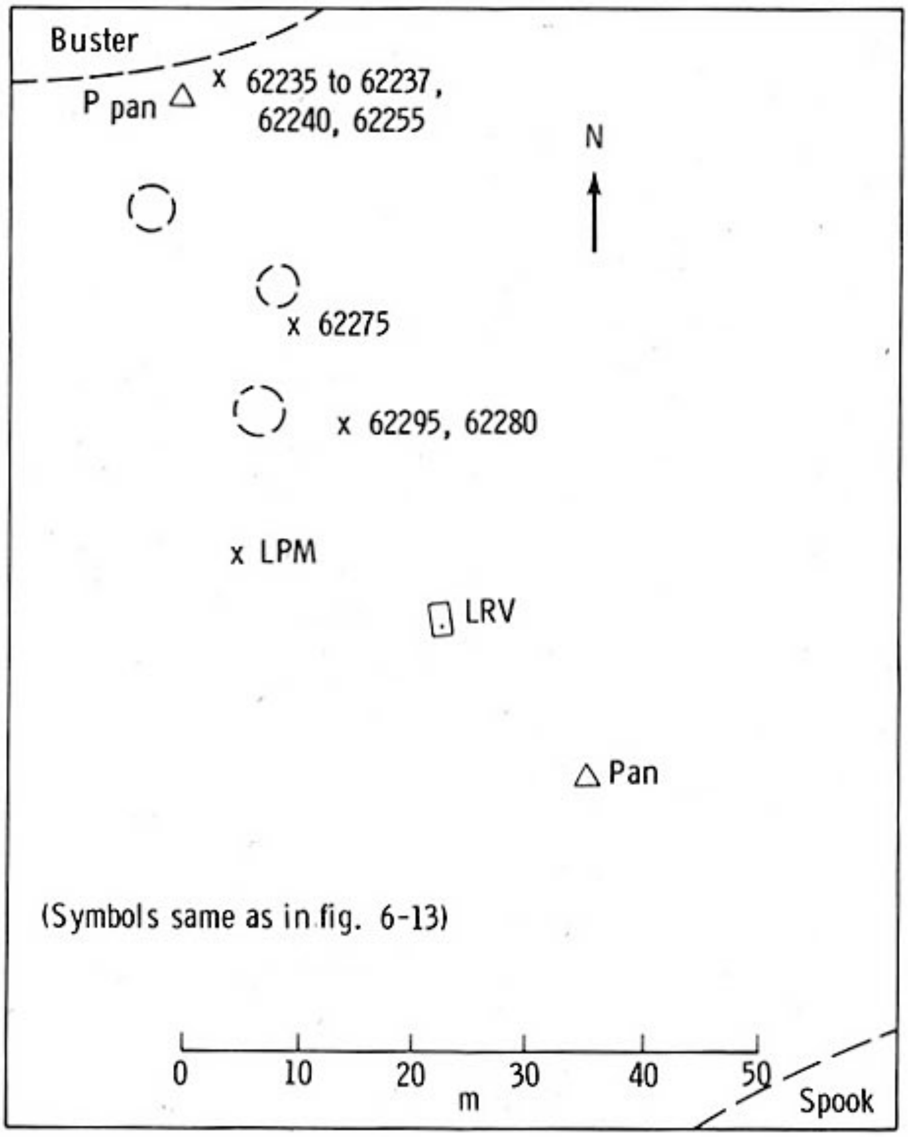

Figure D3 – Planimetric map of Station 2 of EVA 1 [4]

D.1.2.1 Sources: The images used for this study are taken from Apollo 16 Journey to Descartes, complete TV and on-board film © 2005 Spacecraft Film (courtesy NASA). The sequence relating to the collection of sample 62275 is published at this link: https://youtu.be/V3fmK5iJJV0 [*Ann. D1*]

D.1.2.2 Other official sources containing the same sequence:

- Apollo 16 Lunar Surface Journal Corrected Transcript and Commentary by Eric M. Jones 1997, last revised 01 May 2018. https://www.hq.nasa.gov/wp-content/uploads/static/history/alsj/a16/a16v.1243911.mpg [*Ann. D2*]

D.2 Sample bag drop

---

[4] *https://www.hq.nasa.gov/wp-content/uploads/static/history/alsj/a16/as16psr.pdf Apollo 16 Preliminary Science Report, NASA Manned Spacecraft Center, Scientific and Technical Information Office 1972*

Let's start the analysis of this long sequence starting from the two events which result simpler to be tracked, and that temporally follow the more complex and most interesting one. The first of these two events is the vertical fall of the sample bag extracted from its dispenser by Charles Duke at the beginning of the sequence. During the second attempt to collect the Cataclastic Anorthosite 62275, the bag destined for its collection escapes the astronaut's grip, also because he has to hold both the Large Adjustable-angle Scoop and the Sample Bag in his left hand. Pushed by an involuntary throw of the astronaut who was lowering his limb, the bag rotates between Duke's fingers, then hits his wrist, then flips over and falls to the ground.

D.2.1 Lunar Sample Bag [5]

Figure D4 – Documented Sample Bag, Flat

Documented sample bags were used for organizing rock and soil samples. This type of bag was used on Apollo 15-17 and was designed to hold an 11-cm diameter rock. A dispenser held 20 of these bags. After a sample was placed in the bag, the bag was held closed by aluminum tabs.

At the Smithsonian National Air and Space Museum (Washington DC) there are currently two types of Lunar Rock Bags and relative dispensers: a first model with Teflon bags (Figure D4) and a second, very similar model with polyethylene bags (Figure D5).

---

[5] *https://airandspace.si.edu/collection-objects/documented-sample-bag-flat/nasm_A19790810000 Smithsonian National Air and Space Museum, 6th St and Independence Avenue, SW Washington, DC 20560*

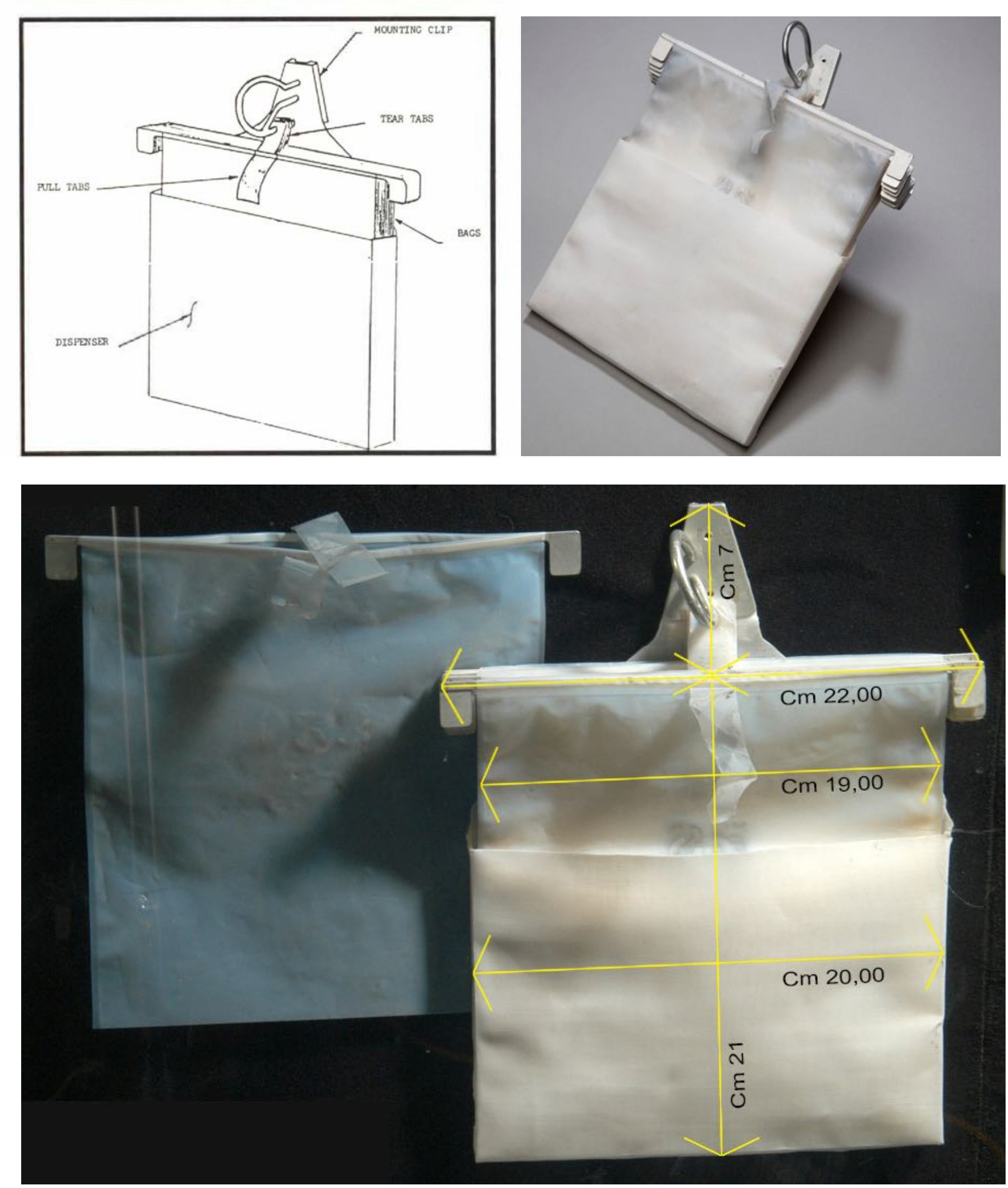

Figure D5 – 20-bag dispenser used by Apollo 15, 16, 17. [6]

Here below are the declared technical data:

---

[6] https://airandspace.si.edu/collection-objects/bag-documented-sample-flat-rectangular-apollo/nasm_A19810920001 *Smithsonian National Air and Space Museum, 6th St and Independence Avenue, SW Washington, DC 20560. This set of flat bags was transferred to the Smithsonian from NASA in 1974.*

Lunar Rock Bag, Teflon

Manufacturer: Union Carbide Corporation; Materials: Teflon, aluminium.

Dimensions: 8 in. long x 7 1/2 in. wide (20.32 x 19.05 cm), weight (single bag): 10.2 g (0.22 lb). The relationship between length and width inferable from Img. 78 confirms that these measurements do not include the mounting clip and the aluminium side flaps present on each bag.

Lunar Rock Bag, Polyethylene

Dispenser: 7 7/8 × 1 15/16 × 11 in. (28 × 5 × 20 cm)

Single bag: 8 11/16 × 1/16 × 8 1/4 in. cm (21 × 0.2 × 22 cm)

In this case, the proposed dispenser length (28 cm) also includes the mounting clip. The measurement of the width of the bags (22 cm) includes the aluminium flaps at both ends.

Considering that the metal parts necessary to close the bags were produced in series it can be assumed that the two sets of bags / dispensers have the same width (19 cm). However, the set with polyethylene bags has a slightly longer length than the Teflon one (21 cm instead of 20.32 cm). The choice of which of the two Lunar Rock Bag types corresponds to the one whose fall to the ground was filmed in this sequence will not be relevant for the purposes of tracing, since the difference in length rests within the experimental error range
($3u$ = +/- 1.5 px = +/- $9.3 \cdot 10^{-3}$ m).

D.2.2 Calculation of the Focal and of the relative geometric aberration

Scale of Figure D3: 50 meters correspond to 297px

Distance lens - subject:
185 px = 31145 mm +/- 84.17 mm
PLSSctv: 1.8 mm +/- 0.07 mm
PLSSmoon: 660 mm

$$F = distance \cdot \frac{PLSS_{ctv}}{PLSS_{moon}}$$

Focal = $31.145 * \frac{1.8}{660}$ = 84.94 mm (+/- 3.53 mm)

Equivalent Focal $Fe = F \cdot \frac{D_S}{D}$

$Fe = 84.9 \cdot \frac{43.3}{16}$ = 229.9 mm (+/- 9.55 mm)

The calculation of the equivalent focal length shows that the scene was shot with a zoom level equal to a fairly strong telephoto lens. The maximum geometric distortion of the lens must therefore be considered, which, according to the technical information available, reached at least 3% in the direction of the pincushion. This aberration is corrected through the Adobe PS CS6 Lens Correction filter with an equivalent percentage of distortion in the direction of the barrel.

Figure D6 – Measurement of PLSS Unity on the CTV sensor

D.2.3 Dynamics and motion analysis; measurement system.

The events described in D.2 suggest that the falling body is not only subject to the force of gravitational attraction: an initial thrust exerted by the astronaut's limb is evident.
The dynamics of the fall, in its initial phases, is also made more complex by the impact with the wrist. The rotating movement of the bag makes the analysis of the first frames of this part of the sequence too complex, due to the difficulty of identifying the centre of mass without knowing the characteristic data of the various materials of the object. Our choice was therefore to trace a point conventionally identified by the intersection of the diagonals of the bag starting from the phase following the rotation, when the bag descends vertically without further complex evolutions.

The original frames of the sequence are archived in *Ann. D3*. Following the conversions described in A.3.6, 17 of these frames were analysed, numbered from 0 to 16 [*Ann. D4*]. From the images, it can be seen that the first frame whose fields show the impact of the bag with the lunar soil is number 15. This frame contains fields photographed in t_{14}, t_{15}, t_{16}, t_{17} (cf. A.3.2) and presents for the first time a reduction of the vertical colour shift effect, proving that Z_{16} and Z_{17} coincide or are in any case very close. This means that the bag touched the ground between t_{16} and t_{17}. In frame 16 (t_{15}, t_{16}, t_{17}, t_{18}) we can observe an even greater reduction in the colour shift effect due to the vertical overlap of at least the 3 sequential fields $Z_{16} = Z_{17} = Z_{18}$. The measure found $Z_{16} = 0{,}103$ m is approximately equivalent to half of the bag length and confirms that the field closest to the impact is that taken in t_{16}. From t_{17} onwards, the object dissipates its kinetic energy by continuing to move on the lunar ground, rolling and moving away from the astronaut as confirmed in frame 17 by the presence of a horizontal colour shift instead of the vertical one. A 1fps video of this sub-sequence is available at this address: https://youtu.be/qUAoYxeB670 [*Ann. D5*]

In tracing the centre of the object, the dimensions of the bag shown in D.2.1 were taken into account. The motion, which appears approximately in front of the camera, has been analysed in its vertical component only. The tool used for the measurements was the Vanishing Point filter of Adobe PS CS6 [*Ann. D6*]. The scale was calibrated starting from the height of the PLSS Unity (Figure D6) and the ground line was identified through frame no. 16 (the first frame containing a field filmed after the impact), in which it is clearly identifiable, revealing itself almost parallel to the shadow line of a nearby rock (Figure D8).

Figure D7 – Calibration of the measuring system

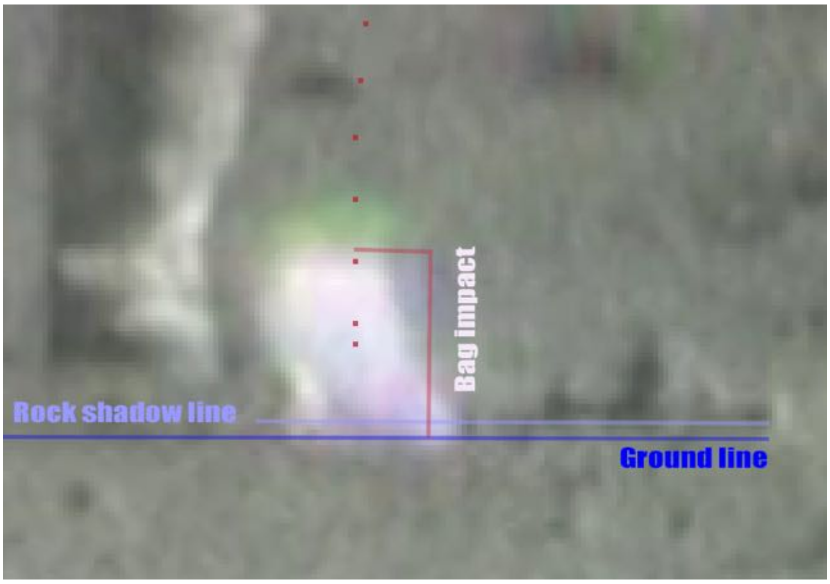

Figure D8 – Identification of the Ground Line based on the first frame following the impact

D.2.4.1 Measurements [*Ann. D7*]

Table D1 here below presents the measurements obtained in relation to the first 16 frames of the sequence to which the hourly law is applicable. We can apply the same considerations made in C.3.7 concerning the experimental error which in this case is equivalent to *3u* = +/- 1.5 px = +/- $9.3*10^{-3}$ m.

The maximum error given by the quadratic sum of instrumental error and accuracy error is shown in the column ErrMax: $ErrMax = \pm \frac{\sqrt{(u^2 + Err^2)}}{2}$

D.2.4.2 Discussion of Results

The fundamental equation of the free fall model on the Z axis is obviously the well-known one:

E_1) $Z_{mod}(t) = Z_0 + (Vz_0 * t) - (\frac{1}{2} * g * t^2)$

Using the Origin Pro 2018 software once again, the fit of the data collected is carried out to verify the model that interprets them more reliably. [*Ann. D8*]

As can be seen from the previous figures D9, D10 and D11, all the tests confirm that the one found by the software is a very effective fit but the result obtained with g = 2.68 m/s^2 suggests that the playing framerate of 29.97 fps is different from the recording framerate.

Frames	T (s)	Z_{bag} (m)	ErrMax (m)
0	0.000	0.9(92)	±0.018
1	0.033	0.9(61)	±0.018
2	0.067	0.9(24)	±0.024
3	0.100	0.8(80)	±0.024
4	0.133	0.8(30)	±0.026
5	0.167	0.7(81)	±0.026
6	0.200	0.7(25)	±0.030
7	0.234	0.6(69)	±0.030
8	0.267	0.6(13)	±0.032
9	0.300	0.5(51)	±0.032
10	0.334	0.4(89)	±0.036
11	0.367	0.4(20)	±0.036
12	0.400	0.3(52)	±0.039
13	0.434	0.2(77)	±0.039
14	0.467	0.2(03)	±0.039
15	0.501	0.1(28)	±0.039

Table D1 – Lunar Rock Bag: Z axis measurements

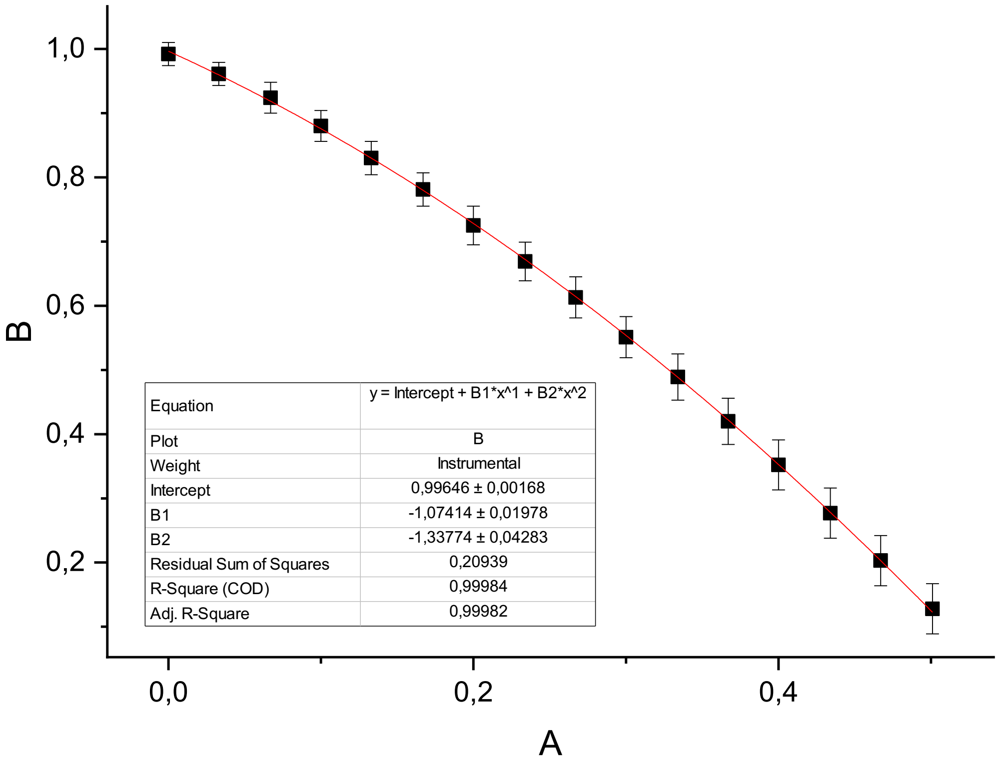

Figure D9 – Fall of the Lunar Rock Bag: fit results plot for the Z-Axis

Equation	y = Intercept + B1*x^1 + B2*x^2
Report Status	New Analysis Report
Weight	Instrumental
Special Input Handling	
Data Filter	No

⊞ *Input Data*

⊞ *Masked Data - Values Excluded from Computations*

⊞ *Bad Data (missing values) -- Values that are invalid and thus not used in computations*

⊟ *Parameters*

		Value	Standard Error	t-Value	Prob>|t|
B	Intercept	0,99646	0,00168	592,48503	0
	B1	-1,07414	0,01978	-54,30231	0
	B2	-1,33774	0,04283	-31,23293	1,29452E-13

Standard Error was scaled with square root of reduced Chi-Sqr.

⊟ *Statistics*

	B
Number of Points	16
Degrees of Freedom	13
Residual Sum of Squares	0,20939
R-Square (COD)	0,99984
Adj. R-Square	0,99982

⊟ *Summary*

	Intercept		B1		B2		Statistics
	Value	Standard Error	Value	Standard Error	Value	Standard Error	Adj. R-Square
B	0,99646	0,00168	-1,07414	0,01978	-1,33774	0,04283	0,99982

⊟ *ANOVA*

		DF	Sum of Squares	Mean Square	F Value	Prob>F
B	Model	2	1313,52339	656,7617	40774,95809	0
	Error	13	0,20939	0,01611		
	Total	15	1313,73278			

At the 0.05 level, the fitting function is significantly better than the function y=constant.

Figure D10 – Fall of the Lunar Rock Bag: fit results for the Z-Axis

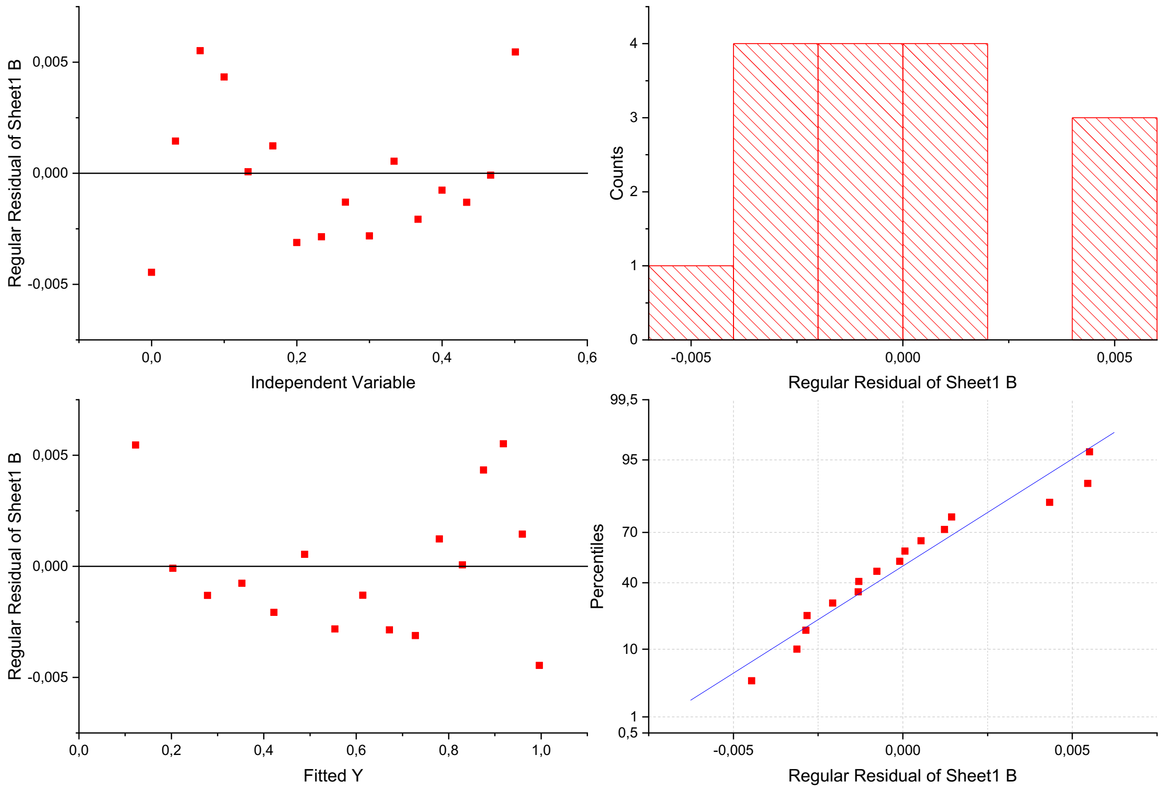

Figure D11 – Fall of the Lunar Rock Bag: fit results for the Z-Axis, study of data variability

D.3 Fall of the Lunar Rock Bags Dispenser

A few moments after the recovery of sample 62275, Charles Duke incurs a second accident: the fall of the entire dispenser of bags used to collect rock samples. The dispenser releases from its seat on the Hasselblad camera for a clumsy manoeuvre by the astronaut, slides for a few moments along his space suit, and then completes its path to the ground in free fall.

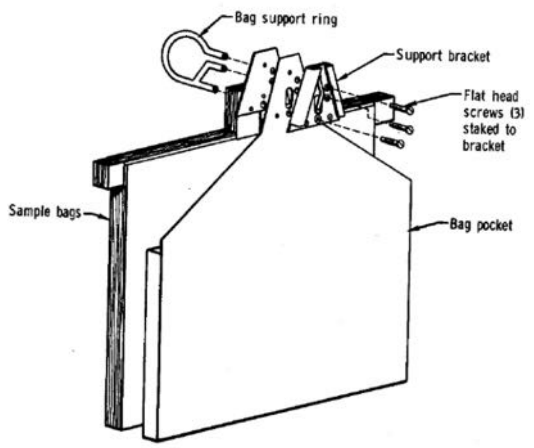

Figure D12 - Documented Sample Bag Dispenser [7]

[7] *https://www.nasa.gov/wp-content/uploads/static/history/alsj/a16/a16mrf14-61.jpg Apollo 16 Lunar Surface Journal https://www.hq.nasa.gov/alsj/a16/a16.sta1.html Corrected Transcript and Commentary Copyright © 1997 by Eric M. Jones. Last revised 7 April 2018*

Figure D13 – Workout position of Sample Bag Dispenser in Apollo 15 [8]

D.3.1 Calculation of the Focal and of the relative geometric aberration

After the event analysed in D.2, the CTV is operated remotely undergoing two different position adjustments and above all a Zoom-Out. For this reason, the calculation of the focal length used must be revised in this new part of the sequence.

Scale of Figure D3: 50 m corresponds to 297px
Lens - subject distance:
185 px = 31.145 mm +/- 84.17 mm

PLSSctv: 1.5 mm +/- 0.02 mm
PLSSmoon: 660 mm

Focal = $31.145 * \frac{1,5}{660}$ = 70.78 mm (+/- 1.13 mm)

Equivalent Focal = $70.78 * \frac{43,3}{16}$ = 191.5 mm (+/- 6.14 mm)

Also in this case we are in the presence of a strong telephoto lens, with a focal length between 185 and 198 mm. In compliance with the applicable technical standards, we therefore consider that the images have undergone the maximum distortion characteristic of CTV: a geometric aberration of 3% in the sense of the

Figure D14 – PLSS Unity measurement in the original sensor scale

[8] *https://www.nasa.gov/wp-content/uploads/static/history/alsj/a15/AS15-90-12233HR.jpg , https://www.nasa.gov/wp-content/uploads/static/history/alsj/a15/AS15-90-12224HR.jpg https://www.hq.nasa.gov/alsj/a15/a15.html Apollo 15 Map and Image Library, Copyright by Eric M. Jones, Last revised 23 November 2016.*

pincushion that we will go to correct in our system.

D.3.2 Dynamics and motion analysis; measurement system.

In this part of the sequence, Astronaut Charles Duke tries to extract a new bag from the dispenser to store the newly collected 62275 rock sample. Three times he gives a push upwards to the dispenser and at the same time causes it to rotate on the horizontal plane counterclockwise. The device oscillates in the two directions described on the anchor pin installed on the Hasselblad camera. At the third energetic solicitation, the dispenser releases from the pin and falls to the ground from a height of about 1.1 m (note that Duke's torso is significantly bent downwards). The constrained rotary motion, triggered by the repeated thrusts received, at the moment of release from the pin, finds the object arranged with the long side parallel to the ground line and it is in this position that it falls to the ground, uncovering its upper side only once the final state of rest is reached. In fact, the object impacts the ground on the side and then lies definitively on its rear surface: only at that moment the aluminium foils placed on the top of the bags and the triangular support that acts as a base for the hook, no longer covered by the rear surface of the object, are highlighted on a plane perpendicular to the rest of the dispenser surface lying on the ground. This “open book” position, compatible with the images shown in Figure 83, is probably due to the flexible structure of the dispenser-bags complex and to the semi-open shape of the container.

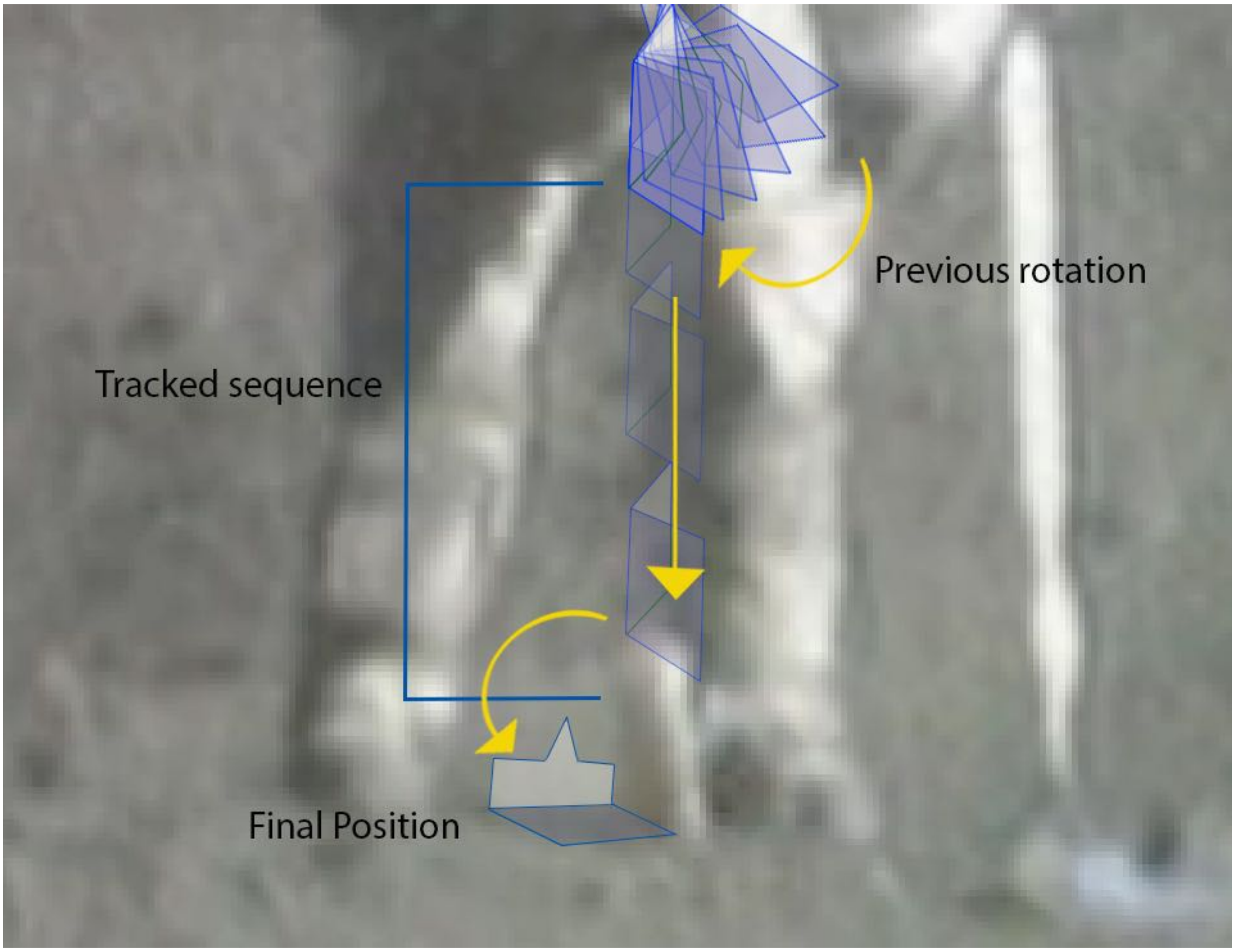

Figure D15 – Description of the overall dynamics of the motion

Unfortunately, even in this case, it has not been possible to analyse the fall of the body in its wholeness, since in the first phase the astronaut's left arm covers almost the entire object. In addition, in the first part of the fall, the object may have rubbed or hit the astronaut's suit, generating friction and therefore slowing down. The metric analyses focused on 20 frames starting from the first frame in which the complete shape of the dispenser is clearly identifiable, about 84 cm from the ground. The fall of the body, which from this moment on proves to be perfectly vertical, made the identification of the centre of mass unnecessary. As in D.2, to carry out the tracking it was in fact preferred to identify a conventional point, as evident as possible. In this case, this point is located at the top of the intersection line of the two perpendicular plans that make up the object. The particular shape assumed by the two surfaces seen from the front and their different colouring (darker the external side and lighter the internal one) have facilitated the measurements and allowed a certain accuracy in identifying the positions they took.

The original frames of the sequence are stored in the *Ann. D9*. Following the conversions described in A.3.6, the 20 analysed frames, numbered from 0 to 19, are available in *Ann. D10*. The frames that first show colour-shift reduction are N. 18 (t_{17}, t_{18}, t_{19}, t_{20}) and N. 19 (t_{18}, t_{19}, t_{20}, t_{21}). This means that the moment closest to the impact with the ground occurs between t_{19} and t_{20}, moments in which the 4 positions of the dispenser within the same frame coincide or are close to coinciding. We can therefore state that the impact occurs about 19 shots after instant 0. The measured value $Z_{19} = 0.2$ m refers to the point drawn at the top of the side facing the plane of view, which agrees with the known width of the dispenser. A 1 fps video of this sequence is available at this address: https://youtu.be/EJ2FSRPuq5M [*Ann. D11*].

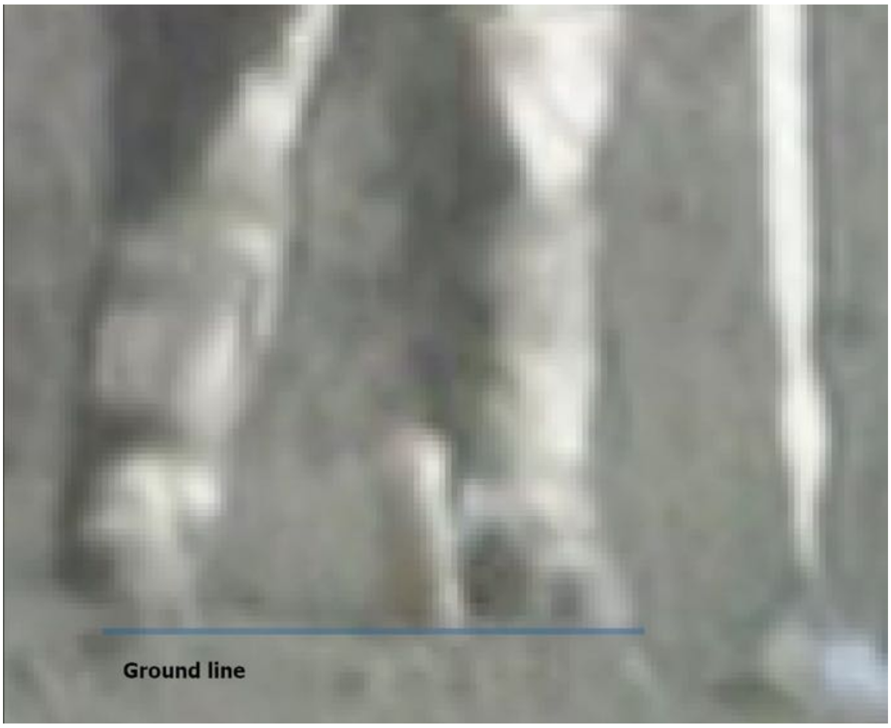

Figure D16 – Identification of the ground line

Also, this time the motion was analysed only in its vertical component and appeared practically in front of the camera. A simplified geometric model was associated with the positions of the falling object in the various frames [*Ann. D12*] in order to facilitate the tracking of the conventional point. Here is the animation of this model at 1fps: https://youtu.be/1IwwLkOAPbc [*Ann. D13*]. The tool used for the measurements was the Perspective Focus filter of Adobe Photoshop CS6. The ground line has been identified starting from N. 19-20-21, in which the surface of the dispenser resting on the ground is clearly evident (Figure D16). The scale was calibrated starting from the width of the PLSS Unity and from the height of the Scoop Extension Handle, thanks to the perfectly vertical position with which the latter is driven into the ground (Figure D17).

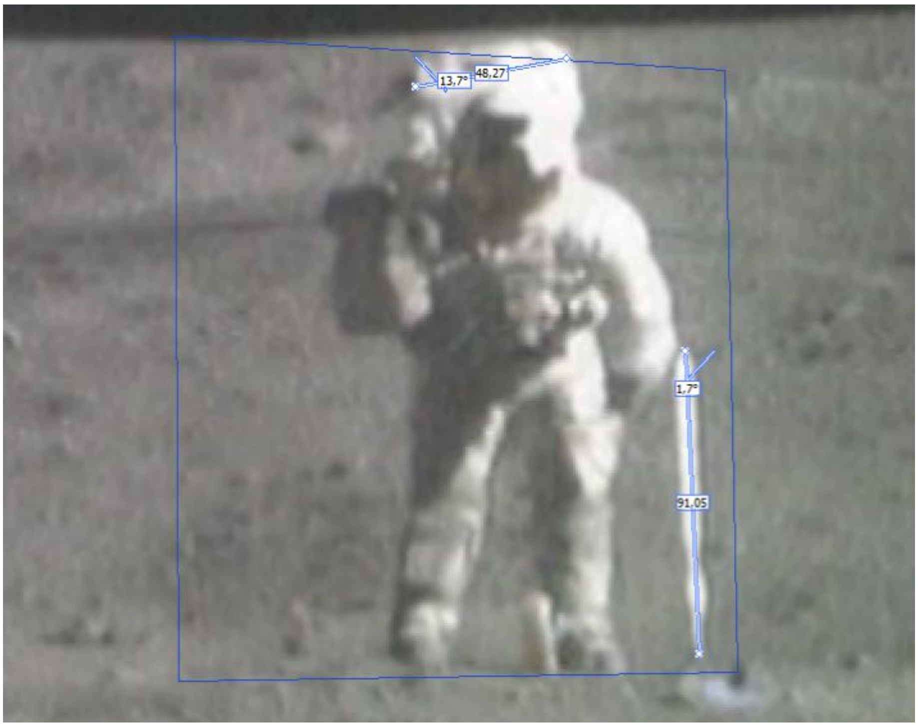

Figure D17 – Calibration of the measuring system

D.3.3.1 Measurements [*Ann. D14*]
Table D2 shows the measurements in meters relating to the position on the Z-axis of the point traced in the 20 frames of the sequence. In this case, the experimental error is $3u$ = +/- 1.5 px = +/- $1.09*10^{-2}$ m. The maximum error $ErrMax = \pm\frac{\sqrt{(u^2 + Err^2)}}{2}$ is reported in the relevant column.

D.3.3.2 Discussion of Results
Given the equation

$E_1)\ Z_{mod}(t) = Z_0 + (Vz_0 * t) - (\frac{1}{2} * g * t^2)$

the fit of the data collected with Origin Pro 2018 is carried out. [*Ann. D15*]

Also in this case the fit identified proves to be effective, as can be ascertained from figures D18 and D19. The value g = 2.82 m/s^2 is consistent with the previous one identified in D.2.4.2 and, since it is far from the admissible values, confirms that the playing framerate of 29.97 fps must be correct.

Frames	T (s)	$Z_{dispenser}$ (m)	ErrMax (m)
0	0.000	0.8(38)	±0.011
1	0.033	0.8(32)	
2	0.067	0.8(16)	±0.013
3	0.100	0.8(01)	
4	0.133	0.7(85)	±0.015
5	0.167	0.7(63)	
6	0.200	0.7(4)	±0.016
7	0.234	0.7(17)	
8	0.267	0.6(87)	±0.019
9	0.300	0.6(57)	
10	0.334	0.6(19)	±0.021
11	0.367	0.5(82)	
12	0.400	0.5(37)	±0.025
13	0.434	0.4(92)	
14	0.467	0.4(39)	±0.029
15	0.501	0.3(86)	
16	0.534	0.3(34)	±0.032
17	0.567	0.2(74)	
18	0.601	0.2(14)	±0.013
19	0.634	0.1(99)	

Table D2 – Bags Dispenser: Z-Axis data

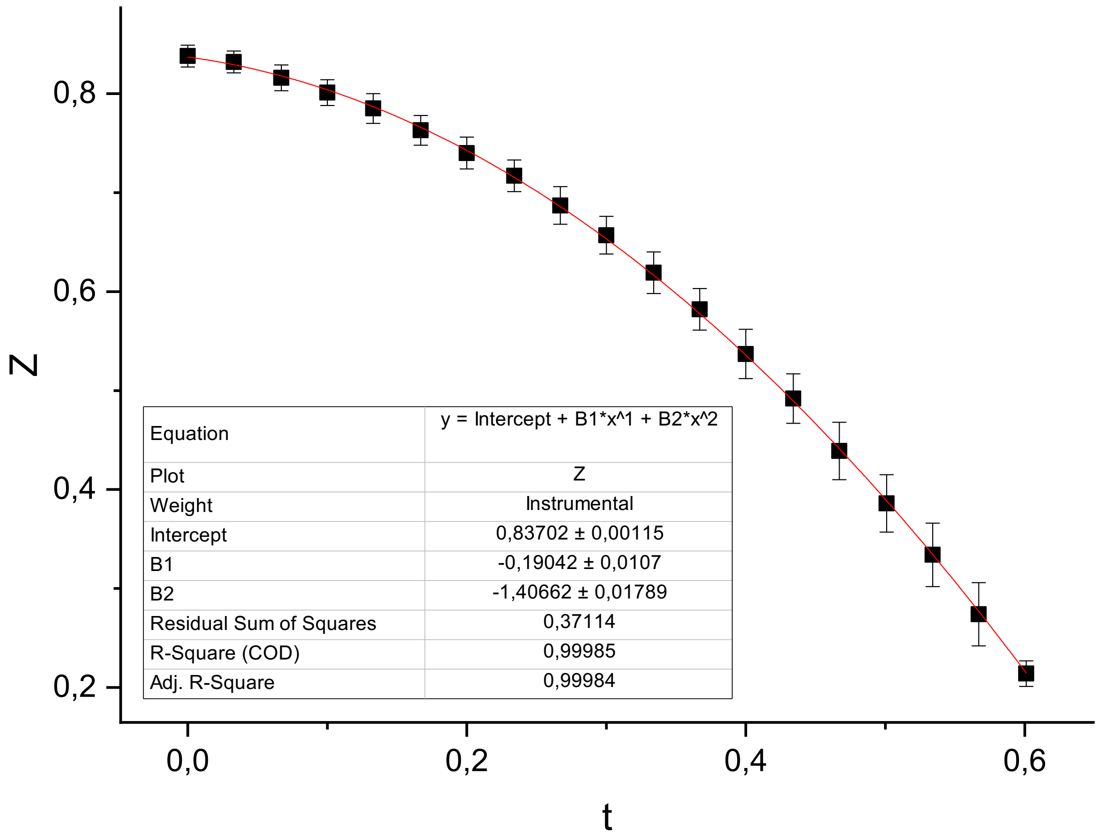

Figure D18 – Fall of the Sample Bag Dispenser: plot of fit results for the Z-Axis

Equation	y = Intercept + B1*x^1 + B2*x^2
Report Status	New Analysis Report
Weight	Instrumental
Special Input Handling	
Data Filter	No

Input Data

Masked Data - Values Excluded from Computations

Bad Data (missing values) -- Values that are invalid and thus not used in computations

Parameters

		Value	Standard Error	t-Value	Prob>|t|
Z	Intercept	0,83702	0,00115	730,75298	0
	B1	-0,19042	0,0107	-17,79572	5,74452E-12
	B2	-1,40662	0,01789	-78,62359	0

Standard Error was scaled with square root of reduced Chi-Sqr.

Statistics

	Z
Number of Points	19
Degrees of Freedom	16
Residual Sum of Squares	0,37114
R-Square (COD)	0,99985
Adj. R-Square	0,99984

Summary

	Intercept		B1		B2		Statistics
	Value	Standard Error	Value	Standard Error	Value	Standard Error	Adj. R-Square
Z	0,83702	0,00115	-0,19042	0,0107	-1,40662	0,01789	0,99984

ANOVA

		DF	Sum of Squares	Mean Square	F Value	Prob>F
Z	Model	2	2546,94068	1273,47034	54899,30895	0
	Error	16	0,37114	0,0232		
	Total	18	2547,31182			

At the 0.05 level, the fitting function is significantly better than the function y=constant.

Figure D19 – Fall of the Sample Bag Dispenser: fit results for the Z-Axis

D.4 Collection of cataclastic anorthosite 62275

A few moments before the fall of the objects we have discussed so far in this section, Charles Duke is busy trying to collect sample 62275, a cataclastic anorthosite of about 440 grams. Due to the usual difficulty of bending and picking up the samples with his hands, Duke performs a sort of juggling (as it is defined by the NASA commentators themselves on *Lunar Surface Journal*) lifting the sample with the scoop and then trying to grab it with his hand, but without succeeding on the first try. The event, filmed by CTV, also involves a small amount of lunar dust presumably collected and launched together with the sample.

D.4.1 The Cataclastic Anorthosite

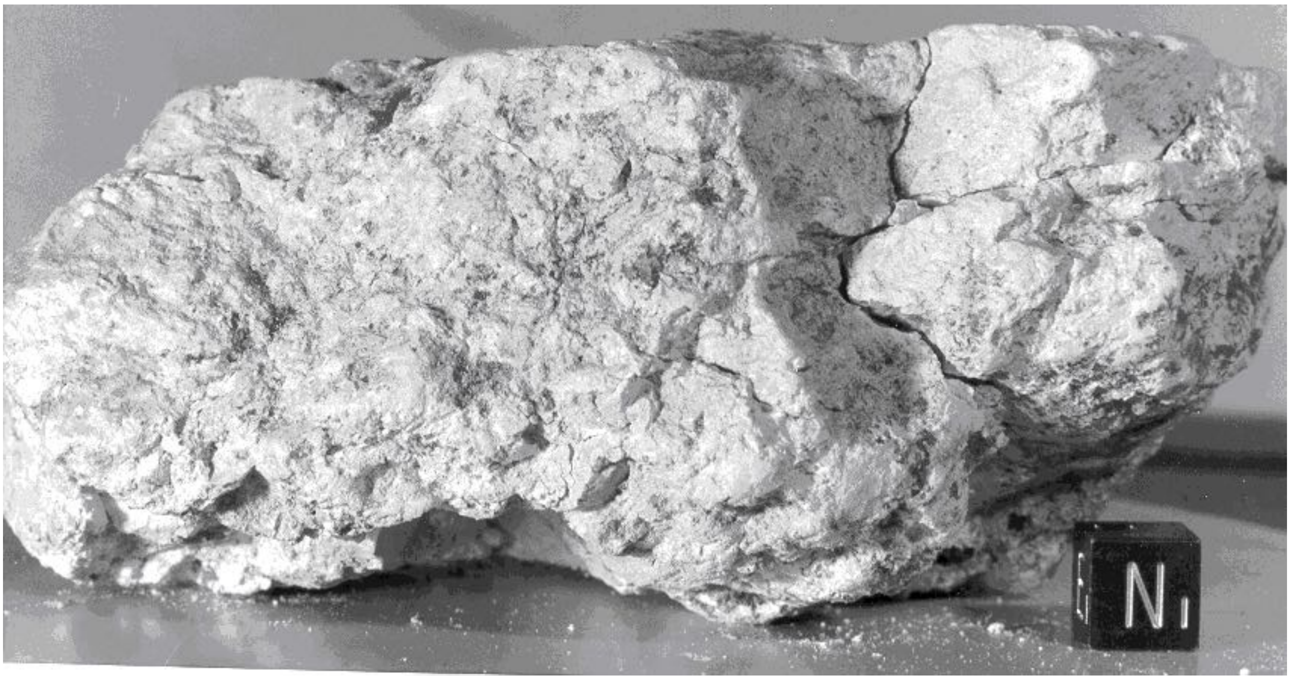

Figure D20 – Sample 62275 of Apollo 16 prior to its fragmentation for analysis purposes

We have already met the anorthosites in the previous section (Big Muley): they are intrusive magmatic rocks that characterize the high lunar lands and the Precambrian shields on Earth. In particular, cataclastic anorthosites denote metamorphic characters caused by exposure to strong pressure. The sample 62275 was found half buried in the regolith near Buster Crater and was thought to be related to ejects from Buster Crater (Sutton 1981). It is a very friable, chalky white rock that broke up into powder during handling in curatorial labs and has not been adequately studied. It appears to be similar to 62236, 62237 and the white portion of 62255, but the plagioclase composition appears more calcic. [9] Its weight, measured on earth, was 443 grams and its maximum dimensions, derived from photometric laboratory images, were approximately: length 11.7 cm; height 6.4 cm; width 8.3 cm. [10]

[9] https://curator.jsc.nasa.gov/lunar/lsc/62275.pdf *Lunar Sample Compendium Charles Meyer - Astromaterials Research & Exploration Science (ARES), NASA 2011, Last Updated: Sep 1, 2016 [Ann. D16]*

[10] http://ser.sese.asu.edu/cgi-bin/DPSC_Data.pl?search=1&rock=62275 *Howard Wilshire and William Phinney, Arizona State University*

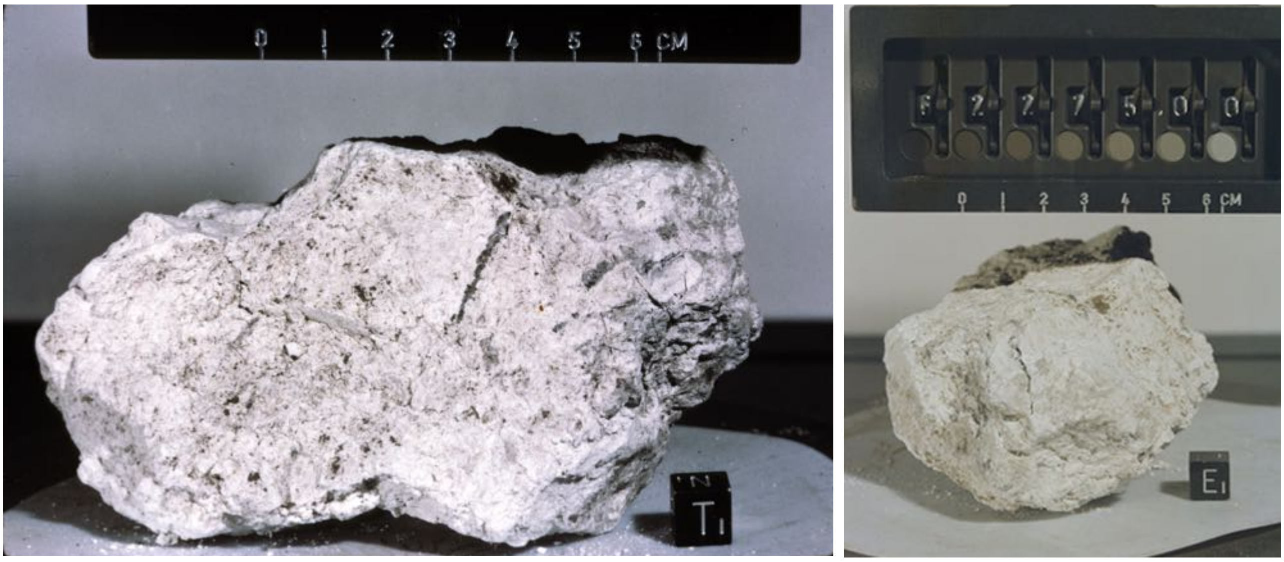

Figure D21 – Photometric images of sample 62275

D.4.1.1 Focal and relative geometric aberration

Between this part of the sequence and the scene analysed in D.2, we note no modifications of the CTV Zoom, therefore we will assume the same focal length calculated in D.2 as the focal used:

Focal = 84.9 mm (+/- 3.53 mm)
Equivalent focal = 229.8 mm (+/- 9.55 mm)

Consequently, an identical aberration of the images equivalent to 3% in the sense of the pincushion is taken into consideration.

D.4.2.1 Dynamics of motion. [*Ann. D17*]

We are faced with a fairly long sequence full of suggestions regarding motion analysis. Astronaut Duke decides to launch up the cataclastic anorthosite 62275 with the aid of the Large Adjustable-angle Scoop and then try to catch it with his hand. This solution will only affect the second and more calibrated attempt in the ambit of which, however, - as we have seen in D.2 - the collection bag will inadvertently escape from his hands and fall to the ground. Here we will take care of tracking the motion of sample 62275 during the first attempt. It is considered the geometric centre of the rectangle in which frame by frame we can inscribe the sample. A motion that was possible to trace with good accuracy for 26 frames. The rock is not the only body to undergo the effect of the kinetic energy impressed by Duke through his scoop: a stripe of lunar dust (regolith), also collected by the scoop, is launched together with the Anorthosite, but it draws a different trajectory compared that of the rock. We consider frame 0 the first frame in which the rock is completely free from the support on the scoop. This occurs when the sample is approximately at the height of the astronaut's forehead: this is the moment in which the astronaut blocks the scoop, giving inertia to the material it contains. From this position, and during 14 frames, the sample will tread about 20 cm in height and then begin the fall towards Duke's glove. Similarly, the head of the dust stripe will detach from the scoop at frame 0 in continuity with the rock (dust and rock are in contact). The head of the dust trail is here tracked, similarly to how we proceeded in section C. The in-depth analysis of the sequence shows that during the upward motion (up to frames 12 and 13), rock and dust tread together, distancing themselves to a very limited extent. During the downward motion, the distance increases significantly. At frame 25 (the last frame detected) the apex of the dust trail is 13.5 cm horizontally and 12 cm vertically far from the closest point of the rock surface. It is possible to see a slow motion of the sequence at 1 fps at this address: https://youtu.be/My2ADS3Pjzo [*Ann. D18*]

D.4.2.2 Measurement system [*Ann. D19*]

The elements of known dimensions used for the calibration system are in this case height and width of the PLSS Unity (see A.2.1.1.2), length of the Extension Handle + Scoop Insertion (see C.4.3), length of the Pan (see C.4.3). For the tracking of the two motions (rock and dust) the plane identified by the Extension Handle and the Pan was used, which is positioned as follows: -32° with respect to the X axis, 18° with respect to the Z axis, -0,5° with respect to the Y axis.

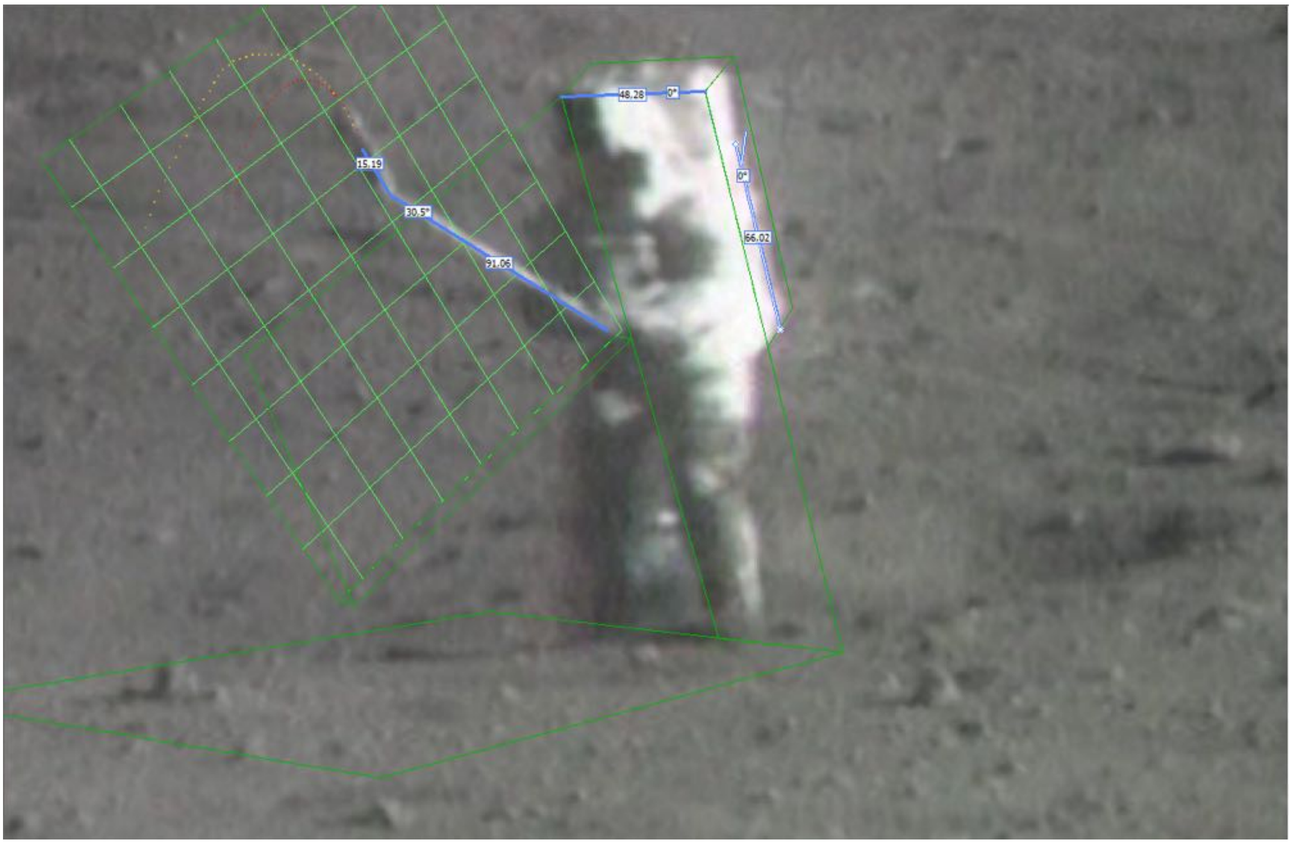

Figure D22 – Calibration of the measuring system

The orthogonal axes X and Z are the first parallel and the second perpendicular to the ground plane. Both axes are positioned appropriately in order to allow us to set measurements with a range suitable for analysis.

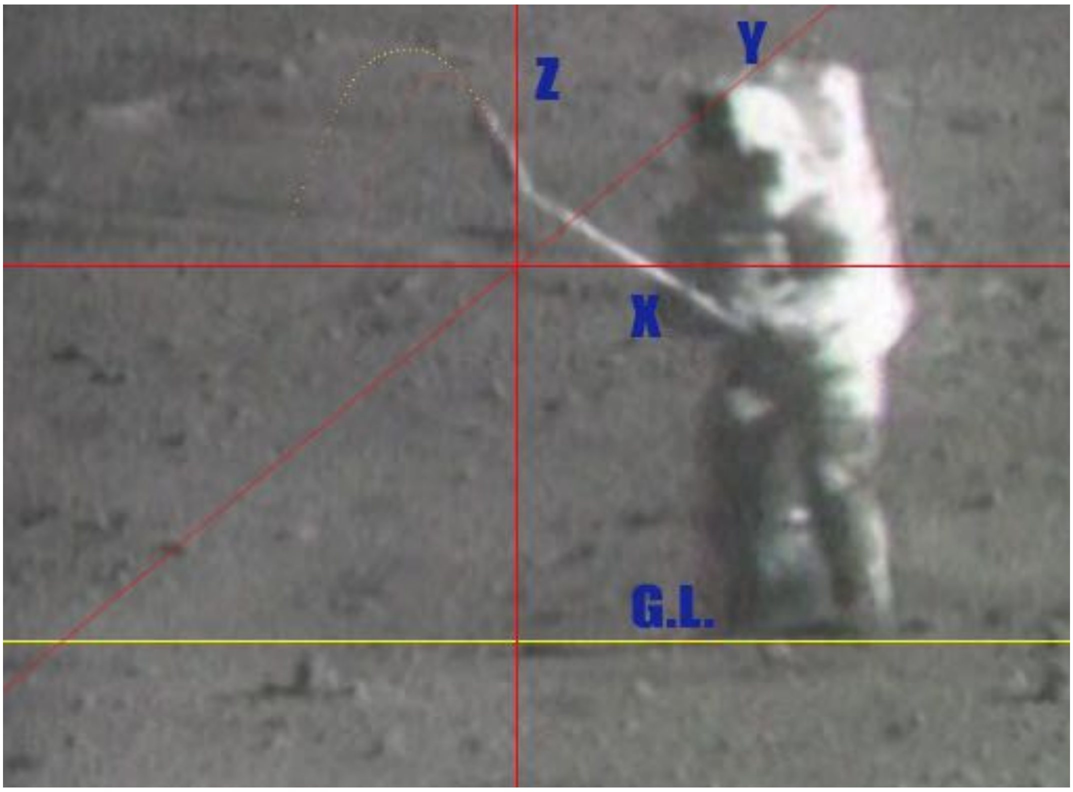

Figure D23 – Positioning of X, Y and Z axis

D.4.3.1 Measurements and results [*Ann. D20*]

The fit from which it is most appropriate to start to exclude the least effective model is of course the one expressed by the motion of the dust. Table D3 reports the measurements in meters taken on the X and Z axes by tracking the motion of the dust which is launched together with the Anorthosite in the 26 frames of the sequence just described. Similarly to what occurred in D.2.4.1, the experimental error in this context is $3u$ = +/- 1.5 px = +/- $9.3*10^{-3}$ m. The maximum error (quadratic sum of instrumental error and accuracy error $ErrMax = \pm\frac{\sqrt{(u^2 + Err^2)}}{2}$) is reported in the specific columns for both X and Z axes.

The fundamental equations of the basic lunar model are the same as seen in the previous sections:

E1) $Z_{mod}(t) = Z_0 + (Vz_0 * t) - (\frac{1}{2} * g * t^2)$ E2) $X_{mod}(t) = X_0 + (Vx_0 * t)$

While the equations of the Earth model are the equally well-known ones:

E3) $X_{airdrag}(t) = X_0 + V_{x0} * \tau * (1 - e^{\frac{-t}{\tau}})$

E4) $Z(t) = Z_0 + (V_{z0} + (g * \tau)) * \tau * (1 - e^{\frac{-t}{\tau}}) - (g * \tau) * t$

Frame	Time (s)	**X (m)**	XErrMax	**Z (m)**	ZErrMax
0	0.000	**0.0(62)**	±0.012	**0.3(64)**	±0.018
1	0.033	**0.0(77)**		**0.3(95)**	
2	0.067	**0.0(92)**	±0.015	**0.4(19)**	±0.015
3	0.100	**0.1(16)**		**0.4(43)**	
4	0.133	**0.1(31)**	±0.012	**0.4(68)**	±0.013
5	0.167	**0.1(46)**		**0.4(86)**	
6	0.200	**0.1(62)**	±0.012	**0.5(11)**	±0.013
7	0.234	**0.1(77)**		**0.5(30)**	
8	0.267	**0.1(92)**	±0.012	**0.5(41)**	±0.011
9	0.300	**0.2(07)**		**0.5(54)**	
10	0.334	**0.2(23)**	±0.012	**0.5(58)**	±0.010
11	0.367	**0.2(37)**		**0.5(64)**	
12	0.400	**0.2(60)**	±0.012	**0.5(69)**	±0.009
13	0.434	**0.2(75)**		**0.5(68)**	
14	0.467	**0.2(90)**	±0.012	**0.5(67)**	±0.009
15	0.501	**0.3(05)**		**0.5(66)**	
16	0.534	**0.3(19)**	±0.012	**0.5(58)**	±0.010
17	0.567	**0.3(33)**		**0.5(51)**	
18	0.601	**0.3(47)**	±0.012	**0.5(38)**	±0.012
19	0.634	**0.3(63)**		**0.5(24)**	
20	0.667	**0.3(77)**	±0.010	**0.5(11)**	±0.011
21	0.701	**0.3(82)**		**0.4(98)**	
22	0.734	**0.3(98)**	±0.012	**0.4(79)**	±0.013
23	0.767	**0.4(12)**		**0.4(60)**	
24	0.801	**0.4(26)**	±0.012	**0.4(34)**	±0.016
25	0.834	**0.4(40)**		**0.4(09)**	

Table D3 – Dust motion tracked on X and Z axes and Maximum Error allowable

Then we use Origin Pro 2018 to analyze the data collected on the two axes. [*Ann. D21*]. Figure D25 shows the results relating to the X-axis according to E_2.

Equation	y = a + b*x
Report Status	New Analysis Report
Weight	Instrumental
Special Input Handling	
Data Filter	No

⊞ *Input Data*

⊞ *Masked Data - Values Excluded from Computations*

⊞ *Bad Data (missing values) -- Values that are invalid and thus not used in computations*

⊟ *Parameters*

		Value	Standard Error	t-Value	Prob>|t|
X	Intercept	0,07026	0,00233	30,20114	0
	Slope	0,45409	0,00465	97,73452	0

Slope is significantly different from zero (See ANOVA Table).
Standard Error was scaled with square root of reduced Chi-Sqr.

⊟ *Statistics*

	X
Number of Points	26
Degrees of Freedom	24
Residual Sum of Squares	5,76519
Pearson's r	0,99875
R-Square (COD)	0,99749
Adj. R-Square	0,99739

⊟ *Summary*

	Intercept		Slope		Statistics
	Value	Standard Error	Value	Standard Error	Adj. R-Square
X	0,07026	0,00233	0,45409	0,00465	0,99739

⊟ *ANOVA*

		DF	Sum of Squares	Mean Square	F Value	Prob>F
X	Model	1	2294,55273	2294,55273	9552,03733	0
	Error	24	5,76519	0,24022		
	Total	25	2300,31792			

At the 0.05 level, the slope is significantly different from zero.

Figure D24 – Throwing of dust behind sample 62275: fit results for the X-axis according to E_2

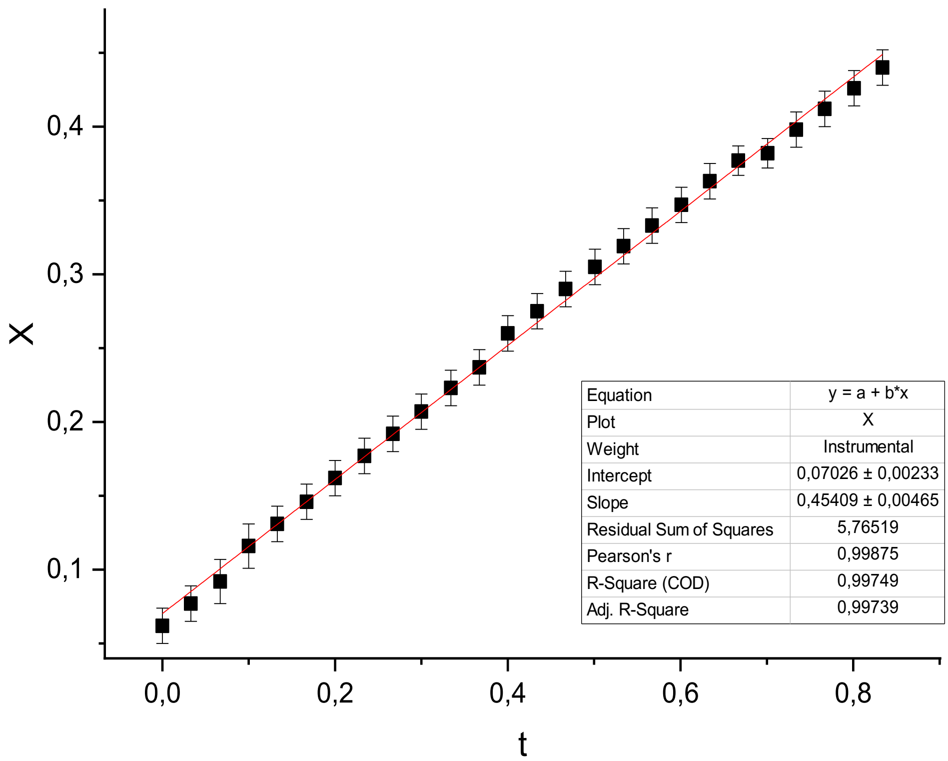

Figure D25 – Dust tracking plot for the X-Axis with fit according to E_2

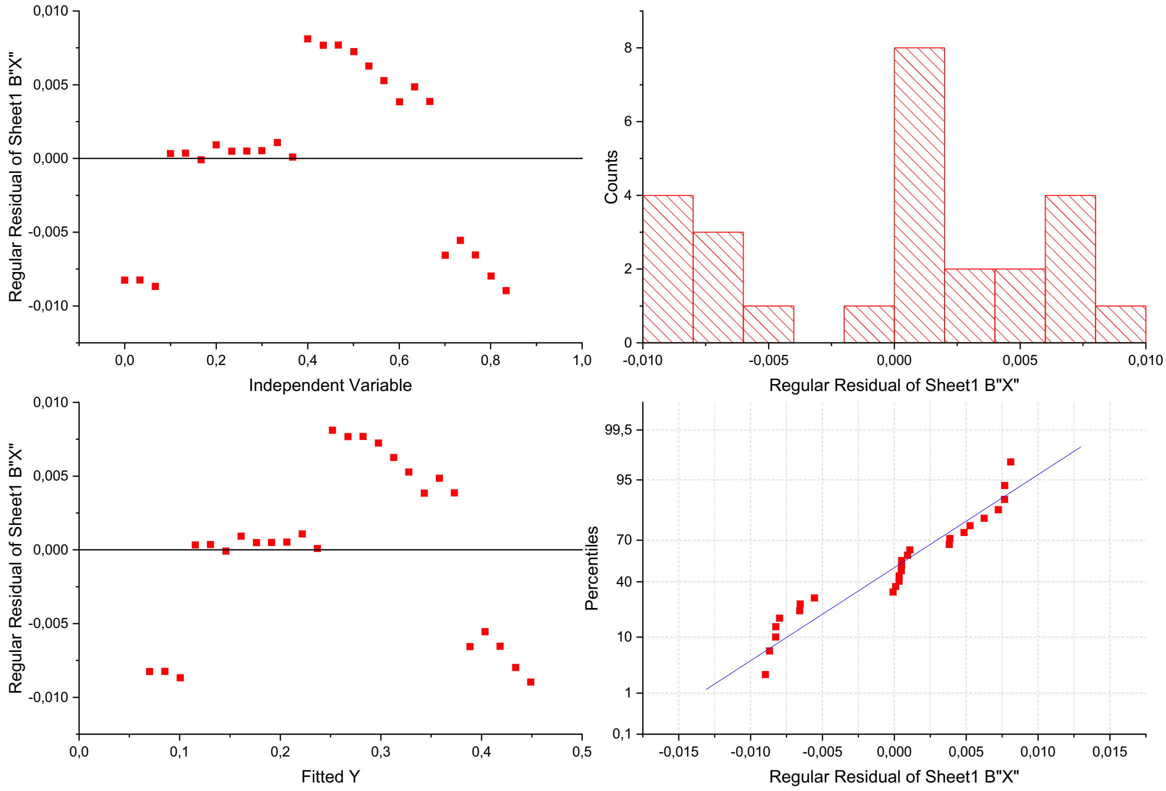

Figure D26 – Data variability Study, X-Axis tracking with fit according to E2

Equation	X = o + v*h*(1 - exp(-t/h))
Report Status	New Analysis Report
Special Input Handling	
Data Filter	No

Input Data

Parameters

		Value	Standard Error	t-Value	Prob>|t|	Dependency
X	o	0,05973	0,00177	33,81314	0	0,88963
	v	0,5331	0,01042	51,16325	0	0,9839
	h	2,58354	0,31384	8,23203	2,61715E-8	0,97105

Reduced Chi-sqr = 0,0625590377196
COD(R^2) = 0,99937449608343
Iterations Performed = 6
Total Iterations in Session = 6
Fit converged. Chi-Sqr tolerance value of 1E-9 was reached.
Standard Error was scaled with square root of reduced Chi-Sqr.

Statistics

	X
Number of Points	26
Degrees of Freedom	23
Reduced Chi-Sqr	0,06256
Residual Sum of Squares	1,43886
R-Square (COD)	0,99937
Adj. R-Square	0,99932
Fit Status	Succeeded(100)

Fit Status Code :
100 : Fit converged. Chi-Sqr tolerance value of 1E-9 was reached.

Summary

	o		v		h		Statistics	
	Value	Standard Error	Value	Standard Error	Value	Standard Error	Reduced Chi-Sqr	Adj. R-Square
X	0,05973	0,00177	0,5331	0,01042	2,58354	0,31384	0,06256	0,99932

ANOVA

		DF	Sum of Squares	Mean Square	F Value	Prob>F
X	Regression	3	15336,48559	5112,16186	81717,39925	0
	Residual	23	1,43886	0,06256		
	Uncorrected Total	26	15337,92444			
	Corrected Total	25	2300,31792			

At the 0.05 level, the fitting function is significantly better than the function X=constant.

Figure D27 – Throwing of dust behind sample 62275: fit results for the X-axis according to E3

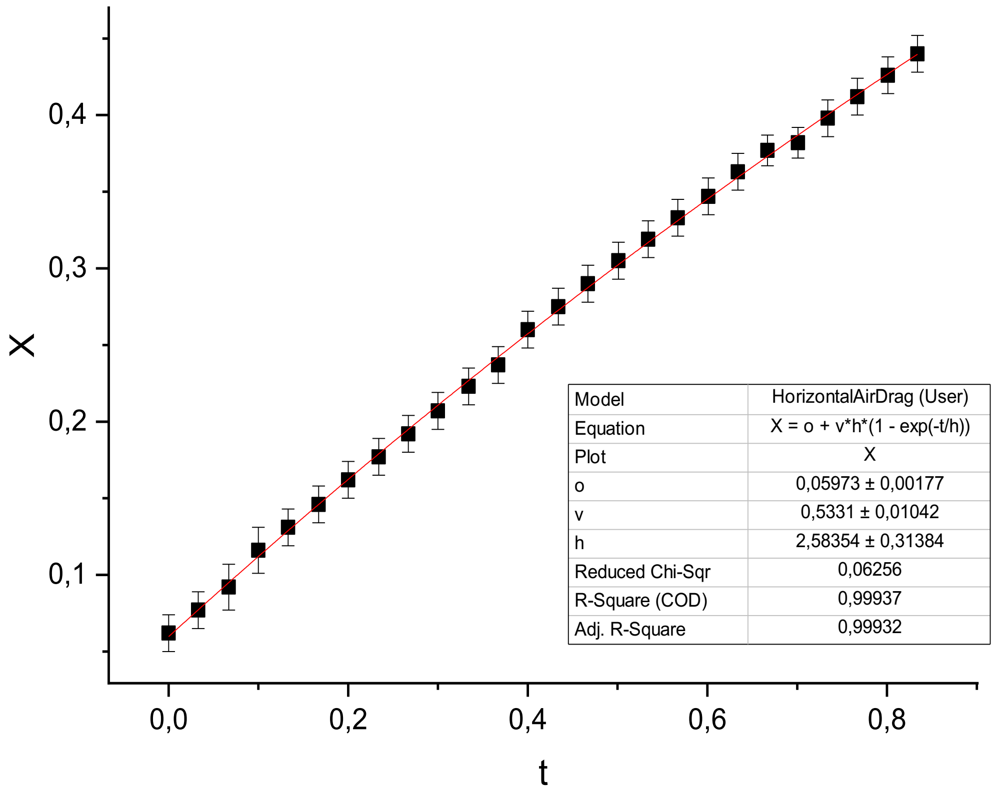

Figure D28 – Dust tracking plot for the X-Axis with fit according to E₃

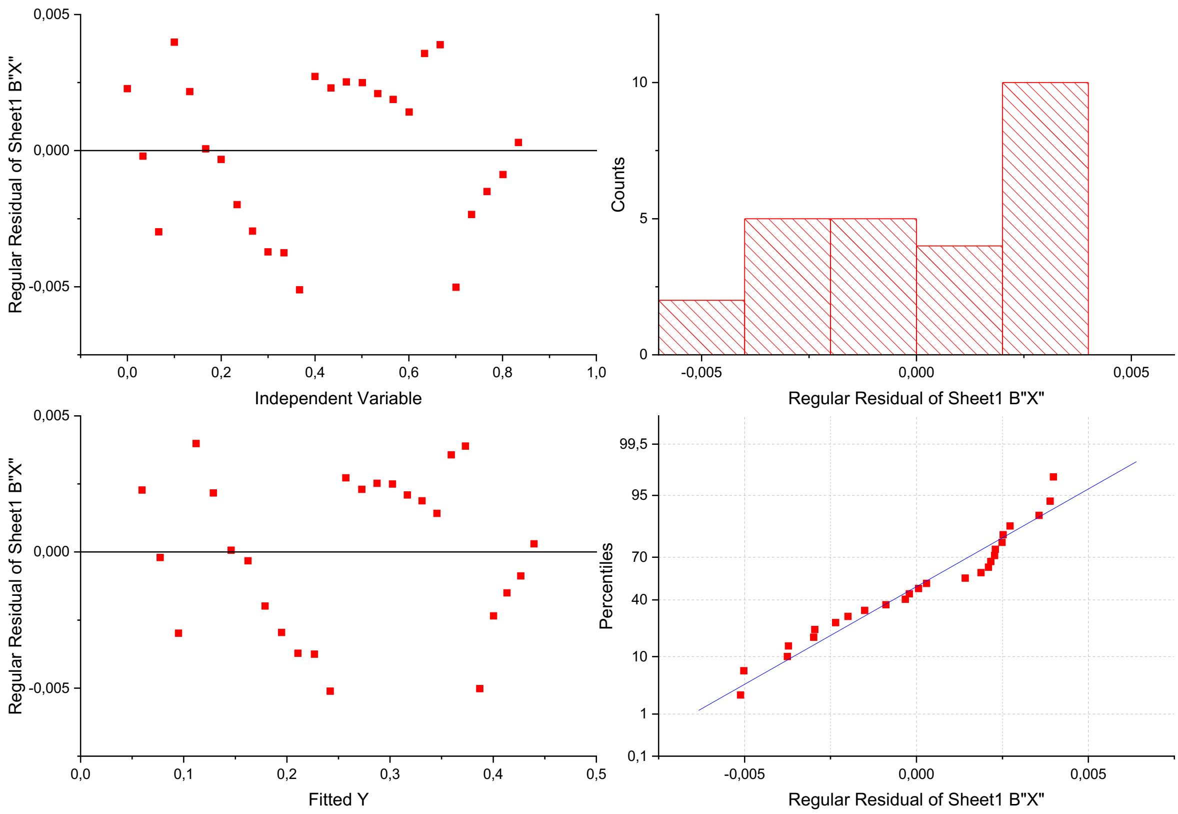

Figure D29 – Data variability Study, X-Axis tracking with fit according to E₃

Fit Comparison of Models

Notes

Description

	Model1	Model2
Input Data	[Book1]Sheet1!(A"t",B"X",C"Xerr")	[Book1]Sheet1!(A"t",B"X",C"Xerr")
Fit Report	[Book1]FitLinear1	[Book1]FitNL1
Equation	y = a + b*x	X = o + v*h*(1 - exp(-t/h))
Function		HorizontalAirDrag (User)
Number of Points	26	26
Number of Parameters	2	3

Preferred Model

	Model Name
AIC	Model2
BIC	Model2
F-Test	Model2

Akaike's Information Criterion Test (AIC)

	RSS	N	Params	AIC	Akaike Weight
Model1	5,76519	26	2	-32,07183	5,95224E-8
Model2	1,43886	26	3	-65,34566	1

Model2 has lower AIC value and so is more likely to be correct.
This model is 1.68004e+007 times more likely to be correct.

Bayesian Information Criterion Test (BIC)

	RSS	N	Params	BIC	Diff BIC
Model1	5,76519	26	2	-29,38845	32,82958
Model2	1,43886	26	3	-62,21803	0

Model2 has lower BIC value and so is more likely to be correct.
BIC difference greater than 10 gives decisive conclusion that Model2 is correct.

F-test

F	Numer.DF	Denom.DF	Prob > F
69,15591	1	23	2,19253E-8

At the 0.05 significance level, Model2 is more likely to be correct.
Note: The F-test results assume the two models are nested.

Figure D30 - X-axis fit, comparison between models E_2 and E_3

As can be seen from Figure D28 and as is easy to deduce from the fits just presented, the E_5 model with air resistance is moderately more effective than the linear one. The software identifies the best time h = τ = 2.58 s.

We then move on to analyze the Z-axis. Figures D31 and D32 present the fits relating to the models expressed by equations E_1 and E_4. In the model with air resistance (E_4) the value of τ just identified with the previous fit was taken into account, imposing it as fixed.

Figure D33 shows that although the two models are very close and although the F-test does not allow a discriminant evaluation, Akaike's Information Criterion Test (AIC) and Bayesian Information Test (BIC) allow us to conclude that the model with air resistance is more likely to be corrected on the Z-Axis as well.

The analysis on the Z axis allows us to identify two other peculiar parameters of the dust motion model: V_{z0} = 0.99 m/s g = 2.10 m/s^2

D.5.1 Discussion of the Section Results

At this point it is legitimate to carry out the framerate correction according to what has already been experimented with in B.3.4.2 and C.4.1 and to take into consideration the hypothesis of a sequence recorded in a terrestrial environment, with g = 9.81 m/s^2. Correct framerate results:

$$fr = 29.97 * \sqrt{\frac{9{,}81}{2{,}10}} = 64.77 \text{ fps}$$

Equation	y = Intercept + B1*x^1 + B2*x^2
Report Status	New Analysis Report
Weight	Instrumental
Special Input Handling	
Data Filter	No

Input Data

Masked Data - Values Excluded from Computations

Bad Data (missing values) -- Values that are invalid and thus not used in computations

Parameters

		Value	Standard Error	t-Value	Prob>|t|
Z	Intercept	0,36491	0,00218	167,28632	0
	B1	0,92879	0,01081	85,93188	0
	B2	-1,05591	0,01223	-86,31107	0

Standard Error was scaled with square root of reduced Chi-Sqr.

Statistics

	Z
Number of Points	26
Degrees of Freedom	23
Residual Sum of Squares	1,56197
R-Square (COD)	0,99696
Adj. R-Square	0,9967

Summary

	Intercept		B1		B2		Statistics
	Value	Standard Error	Value	Standard Error	Value	Standard Error	Adj. R-Square
Z	0,36491	0,00218	0,92879	0,01081	-1,05591	0,01223	0,9967

ANOVA

		DF	Sum of Squares	Mean Square	F Value	Prob>F
Z	Model	2	512,8401	256,42005	3775,7921	0
	Error	23	1,56197	0,06791		
	Total	25	514,40207			

At the 0.05 level, the fitting function is significantly better than the function y=constant.

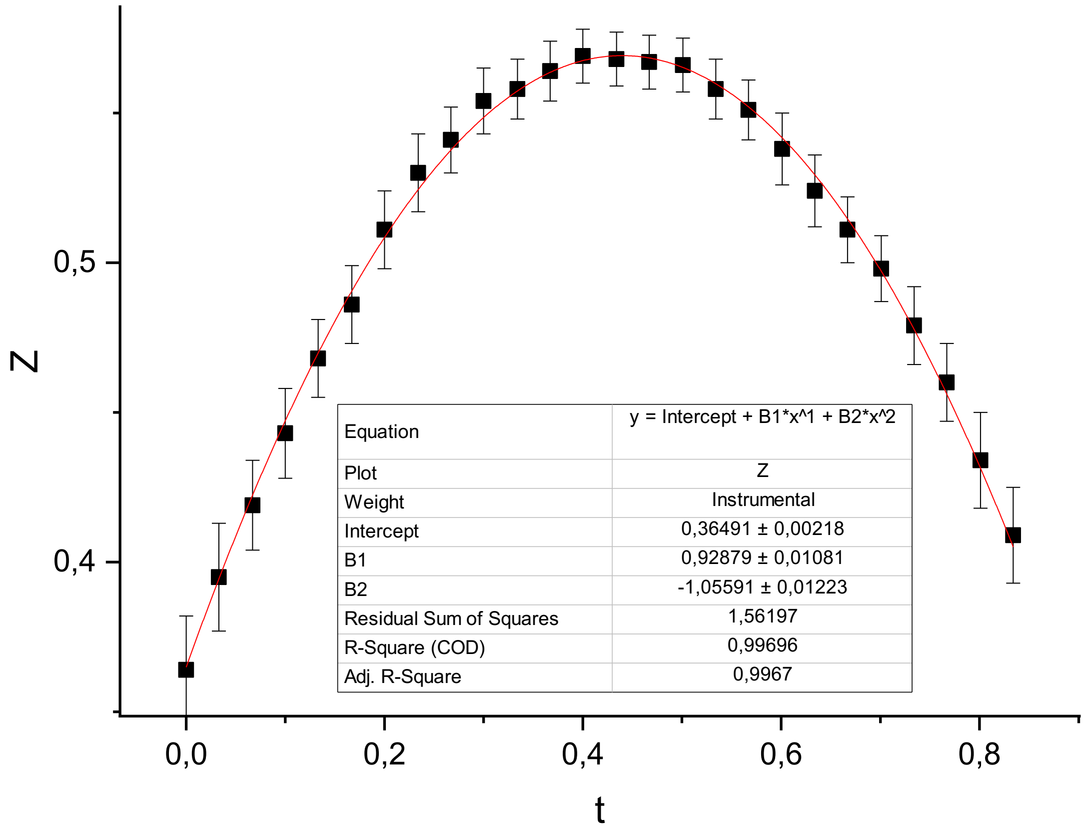

Figure D31 – Dust tracking for the Z-Axis with fit according to E_1

Equation	Z = o + (v+(g*h))*h*(1 - exp(-t/h)) -(g*h)*t
Report Status	New Analysis Report
Special Input Handling	
Data Filter	No

Input Data

Parameters

		Value	Standard Error	t-Value	Prob>|t|	Dependency
Z	o	0,36017	0,00179	201,39699	0	0,92945
	v	0,99112	0,00925	107,14091	0	0,98597
	h	2,58	0	--	--	0
	g	2,09931	0,01968	106,69167	0	0,96902

Reduced Chi-sqr = 0,0439361117087
COD(R^2) = 0,99803552389632
Iterations Performed = 4
Total Iterations in Session = 4
Fit converged. Chi-Sqr tolerance value of 1E-9 was reached.
Some parameter values were fixed.
Standard Error was scaled with square root of reduced Chi-Sqr.

Statistics

	Z
Number of Points	26
Degrees of Freedom	23
Reduced Chi-Sqr	0,04394
Residual Sum of Squares	1,01053
R-Square (COD)	0,99804
Adj. R-Square	0,99786
Fit Status	Succeeded(100)

Fit Status Code :
100 : Fit converged. Chi-Sqr tolerance value of 1E-9 was reached.

Summary

	o		v		h		g		Statistics	
	Value	Standard Error	Value	Standard Error	Value	Standard Error	Value	Standard Error	Reduced Chi-Sqr	Adj. R-Square
Z	0,36017	0,00179	0,99112	0,00925	2,58	0	2,09931	0,01968	0,04394	0,99786

ANOVA

		DF	Sum of Squares	Mean Square	F Value	Prob>F
Z	Regression	3	53869,84805	17956,61602	408698,34215	0
	Residual	23	1,01053	0,04394		
	Uncorrected Total	26	53870,85858			
	Corrected Total	25	514,40207			

At the 0.05 level, the fitting function is significantly better than the function Z=constant.

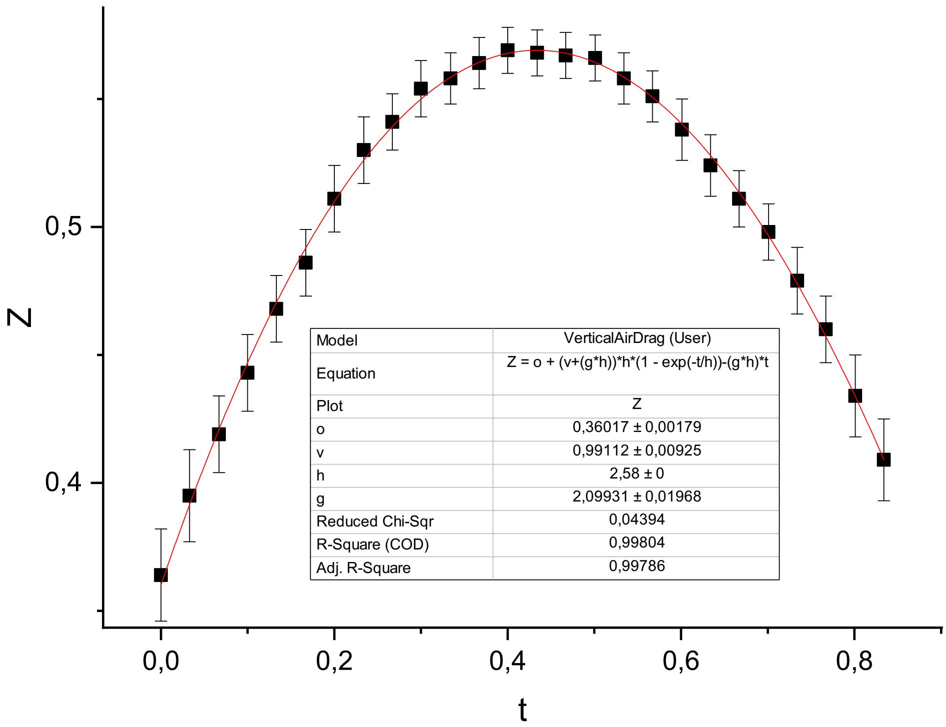

Figure D32 – Dust tracking for the Z-Axis with fit according to E_4

Fit Comparison of Models

Notes

Description

	Model1	Model2
Input Data	[Book1]Sheet1!(A"t",D"Z",E"Zerr")	[Book1]Sheet1!(A"t",D"Z",E"Zerr")
Fit Report	[Book1]FitPolynomial1	[Book1]FitNL2
Equation	y = Intercept + B1*x^1 + B2*x^2	Z = o + (v+(g*h))*h*(1 - exp(-t/h)) -(g*h)*t
Function		VerticalAirDrag (User)
Number of Points	26	26
Number of Parameters	3	3

Preferred Model

	Model Name
AIC	Model2
BIC	Model2
F-Test	No conclusion

Akaike's Information Criterion Test (AIC)

	RSS	N	Params	AIC	Akaike Weight
Model1	1,56197	26	3	-63,21116	0,00347
Model2	1,01053	26	3	-74,53338	0,99653

Model2 has lower AIC value and so is more likely to be correct.
This model is 287.468 times more likely to be correct.

Bayesian Information Criterion Test (BIC)

	RSS	N	Params	BIC	Diff BIC
Model1	1,56197	26	3	-60,08354	11,32222
Model2	1,01053	26	3	-71,40576	0

Model2 has lower BIC value and so is more likely to be correct.
BIC difference greater than 10 gives decisive conclusion that Model2 is correct.

F-test

F	Numer.DF	Denom.DF	Prob > F
--	0	23	--

There is not enough information to draw conclusion

Figure D33 – Z-axis fit, comparison between models E_1 and E_4

Considering the framerate correction factor, the definitive values of initial vertical speed and time τ are the following:

$$\tau' = \frac{2.58}{\sqrt{\frac{9.81}{2.10}}} = 1.19 \text{ s} \qquad V_{z0}' = 0.99 * \sqrt{\frac{9.81}{2.10}} = 2.14 \text{ m/s}$$

Such a value τ' is obtained from a dust particle with the following mechanical characteristics:

Particle Diameter	363	micron
Particle Surface Section	0.103	mm2
Particles Volume	$2.50449*10^{-11}$	m3
Basalt Density	2950	kg/m3
Particle Mass	$7.38823*10^{-8}$	Kg
Coef. Air Viscosity	$1.81000*10^{-5}$	
Sphere Resistance Constant	9.42478	
β	$1.70588*10^{-4}$	
Time τ of Vx for 1/e	1.19312	s

Table D4 – Mechanical characteristics of dust particles

The average diameter of the dust particles tracked in this sequence is therefore approximately 100 microns larger than the one analyzed in section C, but always perfectly compatible with the grain size range deducible from the scientific information available about the Lunar Soil Simulant 4. In the following table D5, we report the measurements relating to the tracking of the Anorthosite 62275 fall according to the equations:

E1) $Z_{mod}(t) = Z_0 + (Vz_0 * t) - (\frac{1}{2} * g * t^2)$ E2) $X_{mod}(t) = X_0 + (Vx_0 * t)$

The data collected on the Z axis are fitted according to the model expressed by equation E_1, as shown in figure D32, taking into account the framerate of 65 fps and imposing: $\frac{1}{2}$ g = - 4.905 m/s^2. [*Ann. D22*]. Considering the minimum confidence threshold of 95%, the model is compatible with the metric values of the tracking.

Frame	Time (s)	**X (m)**	XErrMax	**Z (m)**	ZErrMax
0	0.000	**0.0(62)**	±0.012	**0.3(64)**	±0.015
1	0.015	**0.0(77)**		**0.3(95)**	
2	0.031	**0.0(92)**	±0.015	**0.4(19)**	±0.015
3	0.046	**0.1(16)**		**0.4(43)**	
4	0.062	**0.1(31)**	±0.015	**0.4(68)**	±0.013
5	0.077	**0.1(46)**		**0.4(86)**	
6	0.092	**0.1(62)**	±0.012	**0.5(11)**	±0.013
7	0.108	**0.1(77)**		**0.5(30)**	
8	0.123	**0.1(92)**	±0.012	**0.5(41)**	±0.011
9	0.138	**0.2(07)**		**0.5(54)**	
10	0.154	**0.2(23)**	±0.014	**0.5(58)**	±0.011
11	0.169	**0.2(37)**		**0.5(64)**	
12	0.185	**0.2(60)**	±0.012	**0.5(69)**	±0.01
13	0.200	**0.2(75)**		**0.5(68)**	
14	0.215	**0.2(90)**	±0.014	**0.5(67)**	±0.009
15	0.231	**0.3(05)**		**0.5(66)**	
16	0.246	**0.3(19)**	0.014	**0.5(58)**	±0.009
17	0.262	**0.3(33)**		**0.5(51)**	
18	0.277	**0.3(47)**	±0.014	**0.5(38)**	±0.010
19	0.292	**0.3(63)**		**0.5(24)**	
20	0.308	**0.3(77)**	±0.011	**0.5(11)**	±0.010
21	0.323	**0.3(82)**		**0.4(98)**	
22	0.338	**0.3(98)**	±0.014	**0.4(79)**	±0.011
23	0.354	**0.4(12)**		**0.4(60)**	
24	0.369	**0.4(26)**	±0.012	**0.4(34)**	±0.013
25	0.385	**0.4(40)**		**0.4(09)**	

Table D5 – Sample 62275: data detected on the X and Z axes

Equation	y = A + B*x + C*x^2
Report Status	New Analysis Report
Special Input Handling	
Data Filter	No

⊞ *Input Data*

⊟ *Parameters*

		Value	Standard Error	t-Value	Prob>|t|	Dependency
Z	A	0,39978	0,00468	85,35942	0	0,814
	B	2,16912	0,01991	108,95328	0	0,814
	C	-4,905	0	--	--	0

Reduced Chi-sqr = 0,865930323253
COD(R^2) = 0,95930132288613
Iterations Performed = 3
Total Iterations in Session = 3
Fit converged. Chi-Sqr tolerance value of 1E-9 was reached.
Some parameter values were fixed.
Standard Error was scaled with square root of reduced Chi-Sqr.

⊟ *Statistics*

	Z
Number of Points	26
Degrees of Freedom	24
Reduced Chi-Sqr	0,86593
Residual Sum of Squares	20,78233
R-Square (COD)	0,9593
Adj. R-Square	0,95761
Fit Status	Succeeded(100)

Fit Status Code :
100 : Fit converged. Chi-Sqr tolerance value of 1E-9 was reached.

⊟ *Summary*

	A		B		C		Statistics	
	Value	Standard Error	Value	Standard Error	Value	Standard Error	Reduced Chi-Sqr	Adj. R-Square
Z	0,39978	0,00468	2,16912	0,01991	-4,905	0	0,86593	0,95761

⊟ *ANOVA*

		DF	Sum of Squares	Mean Square	F Value	Prob>F
Z	Regression	2	74052,37821	37026,18911	42758,85497	0
	Residual	24	20,78233	0,86593		
	Uncorrected Total	26	74073,16054			
	Corrected Total	25	510,6389			

At the 0.05 level, the fitting function is significantly better than the function y=constant.

Figure D34 – Results of the fit, tracking of the anorthosite fall, Z axis with g = 9.81 m/s2

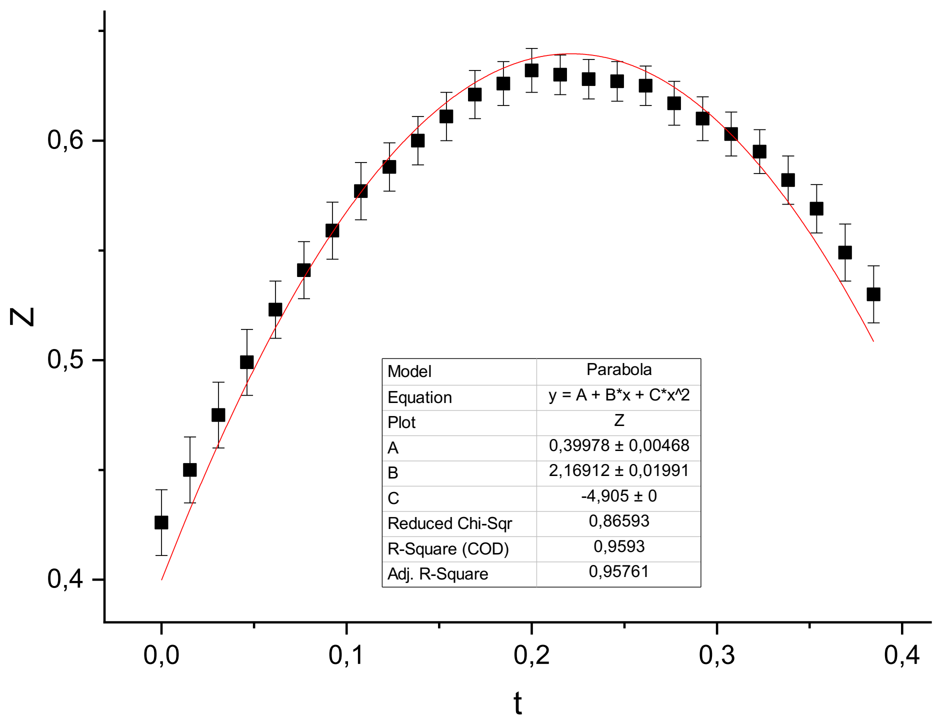

Figure D35 – Plot of the fit, anorthosite fall in a terrestrial environment, Z-axis

Confirmation of the validity of the terrestrial hypothesis is given by the parameter B ($V_{z0\text{-}Rock}$) identified by the Origin Pro fit. The value of 2.17 m/s is almost identical to the homologous one resulting from the fit of the dust motion ($V_{z0\text{-}Dust}$ = 2.14 m/s). If anorthosite and dust received the same initial push, it means that the distance they assume at frame 25 is essentially due to the braking action of the air. In the fits presented below in Figures D33 and D34, we can see how both in the case of the Lunar Sample Bag (D2) [*Ann. D23*] and the Bags Dispenser (D.3) [*Ann. D24*], the hypothesis that the recording of the sequence took place in a terrestrial environment with a framerate of 65 fps is perfectly compatible with the trackings identified on the Z axis.

Equation	y = A + B*x + C*x^2
Report Status	New Analysis Report
Special Input Handling	
Data Filter	No

Input Data

Parameters

		Value	Standard Error	t-Value	Prob>|t|	Dependency
B	A	1,00369	0,00278	360,52335	0	0,56895
	B	-2,61362	0,02652	-98,54909	0	0,56895
	C	-4,905	0	--	--	0

Reduced Chi-sqr = 0,0699988616397
COD(R^2) = 0,99925404612321
Iterations Performed = 3
Total Iterations in Session = 3
Fit converged. Chi-Sqr tolerance value of 1E-9 was reached.
Some parameter values were fixed.
Standard Error was scaled with square root of reduced Chi-Sqr.

Statistics

	B
Number of Points	16
Degrees of Freedom	14
Reduced Chi-Sqr	0,07
Residual Sum of Squares	0,97998
R-Square (COD)	0,99925
Adj. R-Square	0,9992
Fit Status	Succeeded(100)

Fit Status Code :
100 : Fit converged. Chi-Sqr tolerance value of 1E-9 was reached.

Summary

	A		B		C		Statistics	
	Value	Standard Error	Value	Standard Error	Value	Standard Error	Reduced Chi-Sqr	Adj. R-Square
B	1,00369	0,00278	-2,61362	0,02652	-4,905	0	0,07	0,9992

ANOVA

		DF	Sum of Squares	Mean Square	F Value	Prob>F
B	Regression	2	12869,87143	6434,93571	91929,14804	0
	Residual	14	0,97998	0,07		
	Uncorrected Total	16	12870,85141			
	Corrected Total	15	1313,73278			

At the 0.05 level, the fitting function is significantly better than the function y=constant.

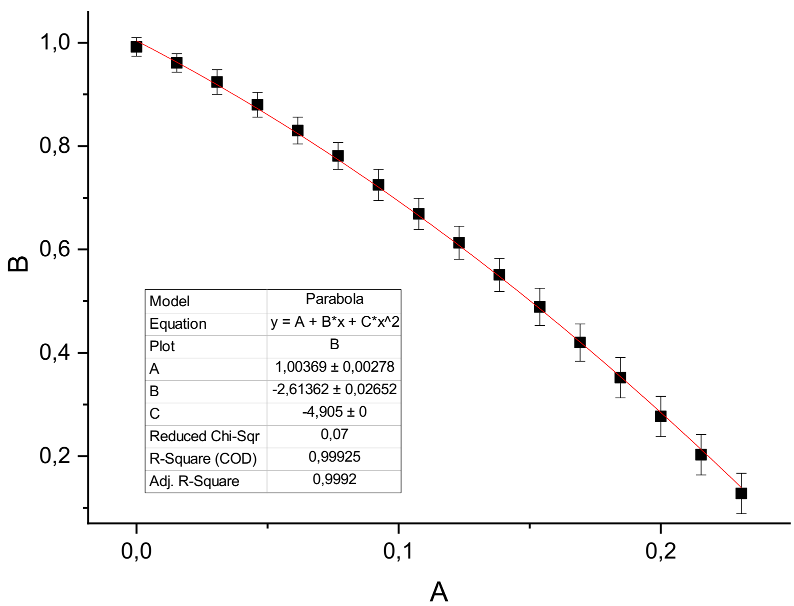

Figure D36 – Fall of the Lunar Sample Bag, fit of the quotas tracked on the Z-axis, framerate 65 fps and g = 9,81 m/s²

Equation	y = A + B*x + C*x^2
Report Status	New Analysis Report
Special Input Handling	
Data Filter	No

Input Data

Parameters

		Value	Standard Error	t-Value	Prob>|t|	Dependency
Z	A	0,85211	0,00444	191,72092	0	0,56101
	B	-0,86652	0,034	-25,48875	5,55112E-15	0,56101
	C	-4,905	0	--	--	0

Reduced Chi-sqr = 0,594786667566
COD(R^2) = 0,99603057102607
Iterations Performed = 3
Total Iterations in Session = 3
Fit converged. Chi-Sqr tolerance value of 1E-9 was reached.
Some parameter values were fixed.
Standard Error was scaled with square root of reduced Chi-Sqr.

Statistics

	Z
Number of Points	19
Degrees of Freedom	17
Reduced Chi-Sqr	0,59479
Residual Sum of Squares	10,11137
R-Square (COD)	0,99603
Adj. R-Square	0,9958
Fit Status	Succeeded(100)

Fit Status Code :
100 : Fit converged. Chi-Sqr tolerance value of 1E-9 was reached.

Summary

	A		B		C		Statistics	
	Value	Standard Error	Value	Standard Error	Value	Standard Error	Reduced Chi-Sqr	Adj. R-Square
Z	0,85211	0,00444	-0,86652	0,034	-4,905	0	0,59479	0,9958

ANOVA

		DF	Sum of Squares	Mean Square	F Value	Prob>F
Z	Regression	2	34572,5472	17286,2736	29062,98097	0
	Residual	17	10,11137	0,59479		
	Uncorrected Total	19	34582,65858			
	Corrected Total	18	2547,31182			

At the 0.05 level, the fitting function is significantly better than the function y=constant.

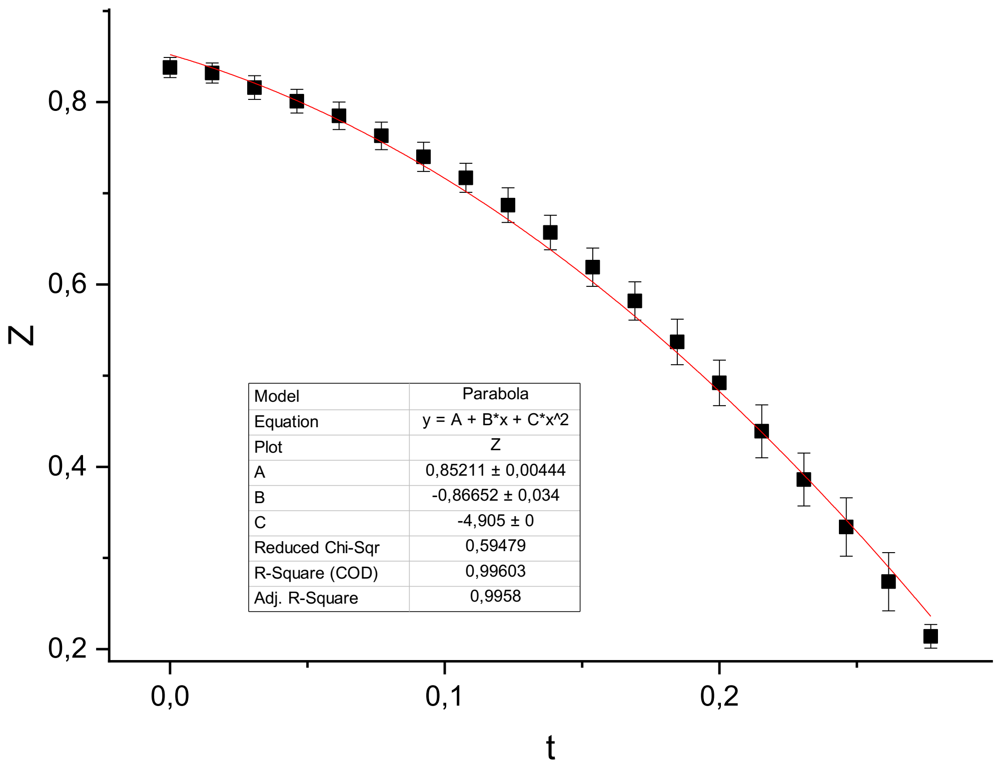

Figure D37 – Fall of the Bags Dispenser, fit of the quotas tracked on the Z axis, framerate di 65 fps e g = 9,81 m/s^2

About the Authors

Alessio Michelotti (ORCID iD: https://orcid.org/0000-0002-3822-104X)
was born in Lucca (IT) the 31-08-72, and obtained a scientific high school diploma at the Liceo Lorenzini in Pescia in 1991 with a specialization in Physics - Mathematics.
He is a professional researcher in the field of Culture with different publications edited by academic publishers in Italy (like Bulzoni Editore and CUEM).

PhD Andrea Simon (ORCID iD: https://orcid.org/0009-0001-3971-4305)
Headmaster in the "Novalis" Italian Waldorf High School where he is also a mathematics and physics teacher, he obtained his Master's Degree in Physics and his teaching qualification from the University of Padua. Among the most significant previous published works is "*First Results of a Scintillating GEM Detector for 2-D Dosimetry in an Alpha Beam*" edited by IEEE in 2008.

Authors contribution

- Alessio Michelotti: Conceptualization, Data curation, Investigation, Project administration, Visualization, Writing – original draft
- Andrea Simon: Conceptualization, Formal Analysis, Methodology, Software, Supervision, Validation

Conflict of interests

The authors declare that there are no conflicts of interest.

ACKNOWLEDGMENTS

Many people, directly and indirectly, have made this study possible through their collaboration. Most of them have not had the opportunity to see the full content of this work, which may be partly outside their respective research fields. Furthermore, the final results of this paper may not reflect, or be in contradiction with, their beliefs or research. However, we would like to thank each of them for their help and for the effectiveness of their valuable contribution.

We would like to thank for their methodological suggestions and encouragement in research: prof. Luis Bilbao, Universidad de Buenos Aires - Departamento de Física; prof. Andrea Simon, Scuola Superiore Novalis, San Vendemiano (Treviso, Italy); prof. Pasquale Bosso, University of Lethbridge (Canada); prof. Derek Bolton, University of Oxford (United Kingdom); Prof. Franco Macchini, University of Pisa (Italy).

This study would not have been possible without the technical information, scientific support and documentary materials provided by:

- James T. Hawes, IT Expert technical, writer & editor
- Mark Gray, Spacecraft Films (Atlanta GA), NASA contractor for Video Editing
- Russ Andersson, SynthEyes, Andersson Technologies LLC (Phoenixville, PA)
- Douglas Brown, Open Source Physics (OSP), Davidson College, Davidson NC, USA

This study has been reviewed by the following researchers:

- **Andreas Märki**, Zurich (CH); Master of Engineering, Swiss Aerospace Industry Technician. Revised sections: Preamble; Sections A, B, C, D.

- Andrea Simon, Vittorio Veneto (IT); Physics teacher and headmaster at Scuola Superiore "Novalis", San Vendemiano (Treviso, IT)**.** Revised sections: Preamble; Sections A, B, C, E.

- **Luis Bilbao**, Buenos Aires (ARG); PhD at the Physics University of Buenos Aires; more than 100 publications in international journals; reviewer for the American Journal of Physics and other major scientific journals. Revised sections: Sections B, E.

- **Dwight Steven-Boniecki**, Köln (DE); Author of Space History: NASA Skylab and Soyuz Mission Reports Editor/Compiler. Revised sections: Preamble; Section A.

- David Chandler, Denver, Colorado (USA); Teacher at Porterville College, Porterville, CA / Physics, Mathematics, and Engineering; publications in American Journal of Physics and other Journals. Served on "The Physics Teacher" Editorial Board as a reviewer.
Revised sections: Preamble.

- **Francesco Vinci**, Avola (IT); Order of Architects P.P.C. Siracusa province; Teacher at Università degli Studi di Catania, Facoltà di Scienze dell'Architettura e dell'Ingegneria Edile. Creator of "Brunelleschi" software for prospective restitution. Revised sections: Preamble; Section A.

Their contribution to the review process is documented in the specific appendix (not attached here).

The previous study "**Analytical Methods for Tracking Bodies Motions on the Lunar Surface in Apollo XVI Footage – *An analysis method*"** has been reviewed as Preprint on the **qeios.com** platform the 22nd April 2024: https://www.qeios.com/read/IA8MXE

The following researchers further revised that work:

Dr. **Jens Biele German** (h-index 36) Aerospace Center (DLR), Köln (DE) – Astronomy, Geophysics, Experimental Physics and Thermodynamics Researcher. Revised sections: Sections A, B, C.

Dr. **Alexey Artamonov** (h-index 9), National Research Nuclear University MEPhI - Moscow Engineering Physics Institute, Moscow (RU). Revised sections: Sections A, B, C.

(English translation by Roberto Leopardi)